Received: 13 July 2023 | Revised: 20 November 2023 | Accepted: 18 December 2023

DOI: 10.1111/gcb.17139

Global Change Biology WILEY

RESEARCH ARTICLE

Persistent net release of carbon dioxide and methane from an Alaskan lowland boreal peatland complex

Eugénie S. Euskirchen[1,2] | Colin W. Edgar[1] | Evan S. Kane[3,4] | Mark P. Waldrop[5] | Rebecca B. Neumann[6] | Kristen L. Manies[5] | Thomas A. Douglas[7] | Catherine Dieleman[8] | Miriam C. Jones[9] | Merritt R. Turetsky[10]

[1]Institute of Arctic Biology, University of Alaska Fairbanks, Fairbanks, Alaska, USA

[2]Department of Biology and Wildlife, University of Alaska Fairbanks, Fairbanks, Alaska, USA

[3]College of Forest Resources and Environmental Science, Michigan Technological University, Houghton, Michigan, USA

[4]Northern Research Station, USDA Forest Service, Houghton, Michigan, USA

[5]U.S. Geological Survey, Geology, Minerals, Energy, and Geophysics Science Center, Moffett Fields, Mountain View, California, USA

[6]Department of Civil and Environmental Engineering, University of Washington, Seattle, Washington, USA

[7]U.S. Army Cold Regions Research & Engineering Laboratory, Fort Wainwright, Fairbanks, Alaska, USA

[8]Department of Integrative Biology, University of Guelph, Guelph, Ontario, Canada

[9]U.S. Geological Survey, Florence Bascom Geoscience Center, Reston, Virginia, USA

[10]Institute of Arctic and Alpine Research, Department of Ecology and Evolutionary Biology, University of Colorado, Boulder, Colorado, USA

Correspondence
Eugénie S. Euskirchen, Institute of Arctic Biology, University of Alaska Fairbanks, Fairbanks, AK, USA.
Email: seeuskirchen@alaska.edu

Funding information
Department of Defense's Strategic Environmental Research and Development Program, Grant/Award Number: RC-2110; National Science Foundation, Grant/Award Number: 0425328, 0724514, 0830997, 1354370 and 2011257; US Geological Survey Climate R&D, Grant/Award Number: RWO 224 and RWO 251; US Forest Service Northern Research Station; U.S. Army Corps of Engineers Engineer Research and Development Center's Basic Research (6.2) Program, Grant/Award Number: 0602182

Abstract

Permafrost degradation in peatlands is altering vegetation and soil properties and impacting net carbon storage. We studied four adjacent sites in Alaska with varied permafrost regimes, including a black spruce forest on a peat plateau with permafrost, two collapse scar bogs of different ages formed following thermokarst, and a rich fen without permafrost. Measurements included year-round eddy covariance estimates of net carbon dioxide (CO_2), mid-April to October methane (CH_4) emissions, and environmental variables. From 2011 to 2022, annual rainfall was above the historical average, snow water equivalent increased, and snow-season duration shortened due to later snow return. Seasonally thawed active layer depths also increased. During this period, all ecosystems acted as slight annual sources of CO_2 (13–59 g C m^{-2} $year^{-1}$) and stronger sources of CH_4 (11–14 g CH_4 m^{-2} from ~April to October). The interannual variability of net ecosystem exchange was high, approximately ±100 g C m^{-2} $year^{-1}$, or twice what has been previously reported across other boreal sites. Net CO_2 release was positively related to increased summer rainfall and winter snow water equivalent and later snow return. Controls over CH_4 emissions were related to increased soil moisture and inundation status. The dominant emitter of carbon was the rich fen, which, in addition to being a source of CO_2, was also the largest CH_4 emitter. These results suggest that the future

carbon-source strength of boreal lowlands in Interior Alaska may be determined by the area occupied by minerotrophic fens, which are expected to become more abundant as permafrost thaw increases hydrologic connectivity. Since our measurements occur within close proximity of each other (≤1 km^2), this study also has implications for the spatial scale and data used in benchmarking carbon cycle models and emphasizes the necessity of long-term measurements to identify carbon cycle process changes in a warming climate.

KEYWORDS
boreal lowland ecosystems, carbon cycling, Interior Alaska, methane emissions, net ecosystem exchange, precipitation, thawing permafrost

1 | INTRODUCTION

Northern peatlands cover 3.7 ± 0.5 million km^2 and store large amounts of carbon (C), with recent estimates of 415 ± 150 Pg C or approximately 80% of the global peatland C stocks (Hugelius et al., 2020). Nearly half of these northern peatlands contain surface permafrost, which is susceptible to degradation and thaw as soils warm under a changing climate (Loisel et al., 2020). Given the large quantity of C stores vulnerable to warming, permafrost peatlands represent a key component of future carbon-climate feedbacks (Natali et al., 2021). While long considered a sink of atmospheric carbon dioxide (CO_2), permafrost peatlands can transition to a CO_2 source upon thaw. In addition, net emissions of methane (CH_4) increase in the initial decades following thaw (Christensen et al., 2007; Frolking et al., 2011; Heffernan et al., 2022; Helbig, Chasmer, Desai, et al., 2017; Helbig, Chasmer, Kljun, et al., 2017). However, the magnitude of this feedback is uncertain, and is regulated by permafrost properties, hydrology, and vegetation (Camill et al., 2001; Helbig, Chasmer, Desai, et al., 2017; Helbig, Chasmer, Kljun, et al., 2017; Schuur et al., 2022).

In the boreal region of Alaska, peatlands encompass 574,000 km^2 or 42% of the boreal landscape (Douglas et al., 2014). These peatlands are comprised of a mosaic of ecosystem types underlain by discontinuous permafrost with dominant cover types including birch, black spruce, mixed and scrub forest and fen and bog meadows. A widespread landscape feature is the peat plateau or ice-rich permafrost peatlands, typically with black spruce cover that are elevated above wetter, unfrozen portions of the landscape (Jorgenson et al., 2022; Zoltai, 1972). When this ice-rich permafrost thaws, ground subsidence catalyzes formation of thermokarst features called collapse scar bogs (Jorgenson et al., 2001, 2010). These bogs become inundated, with visible tree dieback, and are colonized by pioneer mosses, such as *Sphagnum riparium*, and sedge species (Jorgenson & Osterkamp, 2005; Zoltai, 1993). Collapse scar bogs eventually undergo succession, with peat accumulating above the water table and eventually colonization by species adapted to drier conditions (Turetsky et al., 2020). Over periods of several hundred years and under suitable climatic conditions, permafrost may redevelop (Shur & Jorgenson, 2007).

Another common peatland type in boreal regions are rich fens, which often have complex groundwater hydrology and can be too wet and warm to support permafrost formation (Jorgenson et al., 2020). They receive hydrologic inputs from surface or groundwater sources that have been in contact with mineral soils, leading to higher pH and elevated nutrient concentrations compared to poor fens or ombrotrophic bogs, which receive only atmospheric precipitation inputs or runoff from peat plateaus. However, over time and with increasing permafrost thaw, collapse scar bogs may expand outward, becoming hydrologically connected to one another and with local and regional groundwater sources (Quinton et al., 2011), transitioning into fens.

In North American peatlands, including the lowland Tanana Flats region in Interior Alaska (263,964 ha), permafrost attained its maximum extent during the Little Ice Age (Overpeck et al., 1997; Treat & Jones, 2018; Zoltai, 1993). During periods with a relatively warm climate, including the mid-1700s and 1900s as well as the most recent decades, permafrost degradation occurs in this region, resulting in landscape transition (Jorgenson et al., 2001). Jorgenson et al. (2001) found an increase in fen area by 29% between 1949 and 1995. More recently, Lara et al. (2016) estimated a loss of ~7% (15 km^2) of birch forests over the 60 years from 1950 to 2009 due to thermokarst, most of which occurred between warm periods in 1980–1989 and 2000–2009 (Lara et al., 2016). This loss of birch forests resulted in an associated gain in wetland extent. As this landscape transformation continues, we expect C cycling processes within the landscape will also change.

Carbon storage in peatlands occurs because C inputs to the soils from photosynthesis are greater than C losses from microbial and plant respiration (Charman et al., 2013; Gorham, 1991). The difference between gross primary productivity (GPP) and ecosystem respiration (ER) is represented by net ecosystem exchange (NEE, where a positive value represents a net source and a negative value represents a net sink of CO_2), typically with interannual variability in net ecosystem exchange of CO_2 of ~±50 $g\,C\,m^{-2}\,year^{-1}$ (Alekseychik et al., 2021; Baldocchi et al., 2018). Warmer temperatures and increases in atmospheric CO_2 concentration can promote plant growth, increasing GPP (Launiainen et al., 2022; Liu et al., 2019; Ueyama et al., 2020). However, GPP may also be suppressed under hot and dry conditions (Euskirchen

et al., 2014; Olefeldt et al., 2017; Zona et al., 2023). Furthermore, counterbalancing increases in GPP are elevated ER rates, including both plant respiration (Heskel et al., 2016) and soil respiration as microbial activity is stimulated with rising soil temperatures and deeper seasonal thaw into the top of near-surface permafrost, promoting CO_2 release (Laine et al., 2019; Lund et al., 2010; Ueyama et al., 2014). Moisture regimes may also play a role in ER, which can be reduced under both extremely dry (Euskirchen et al., 2014) and inundated conditions (Davidson & Janssens, 2006; Virkkala et al., 2021). Furthermore, the amount of snow in the winter, which is commonly measured through snow water equivalent (SWE), may be related to winter respiration rates (Yi et al., 2015), with deeper snow insulating the ground and warming underlying soils, thereby stimulating microbial activity and release of CO_2 to the atmosphere.

Mechanisms of CH_4 release in boreal peatlands include plant transport, ebullition, and diffusion from soils, all of which are mediated by environmental conditions (Knox et al., 2021). With a wetter landscape undergoing permafrost thaw (Jorgenson & Osterkamp, 2005), combined with forecasted increases in precipitation as both rain (Lehmann & Coumou, 2015; Tebaldi et al., 2006) and snow (Euskirchen et al., 2016), CH_4 emissions may rise. This rise may be due to an increase in methanogenesis as plants that transport CH_4, such as sedges, flourish (Christensen et al., 2004; Turner et al., 2020) or due to other factors such as temperature increases and shifting microbial communities (Waldrop et al., 2023). The magnitude of CH_4 emissions in some boreal peatlands, such as fens and bogs, may also be related to inundation sources, which include spring melt and summer rainfall (Euskirchen et al., 2020; Neumann et al., 2019) as well as possible oxidation by methanotrophs (Zhang et al., 2021). While uncertainty remains and data evaluation techniques are ongoing (i.e., Deventer et al., 2019; Nakai et al., 2020), the introduction of low-power CH_4 instrumentation that can make continuous measurements of CH_4 emissions at an ecosystem level in remote areas (e.g., McDermitt et al., 2011) is providing us with a better understanding of how boreal peatland CH_4 emissions can vary from year to year (Pugh et al., 2017), and the environmental controls on this interannual variability (Delwiche et al., 2021; Knox et al., 2021).

In June 2010, we began measurements of carbon, water, and energy exchange across sites that vary in their presence and stability of permafrost thaw in a lowland boreal landscape of Interior Alaska known as the Tanana Flats (Euskirchen et al., 2014). We chose sites representative of these boreal lowlands that represent a gradient in permafrost thaw without specifically targeting sites undergoing rapid change. Sites include (1) a black spruce forest on a peat plateau with cold soils and stable permafrost, (2) a collapse scar bog formed by thermokarst approximately 100 years ago, (3) a late successional collapse scar bog formed by thermokarst approximately 500 years ago, and (4) a rich fen without permafrost. The landscape represented by these three ecosystem types (black spruce, bog, and fen) are approximately 25%, 7%, and 31% of the 2640 km^2 Tanana Flats region, respectively (Jorgenson et al., 2001). The sites are accessible by road in the snow-free season and with a snow machine during the period of snow-covered ground. They are also in close proximity (<2 km apart) and are therefore under the same climatic regime. We do not include in our measurements the upland boreal ecosystems of Interior Alaska, which contain white spruce and aspen forests on south-facing slopes without permafrost and upland black spruce forests in north-facing slopes with permafrost (Jorgenson et al., 2010).

During our decadal measurement period, the sites experienced impacts of climate warming, including weather-related extreme events. Clear shifts in climate occurred during our study period according to the Köppen climate classification for Fairbanks, AK, which changed from the subarctic category to warm summer continental in 2021 triggered by the mean monthly temperature in May rising above 10°C (NOAA, 2021). Extreme weather events have included extreme warmth, extreme rainfall, and the earliest snowmelt over a 100-year record. A typical summer in Fairbanks has a mean of 3 days with air temperature ≥29°C (NOAA, 2021). However, in 2013, there were 14 days with air temperature ≥29°C (Euskirchen et al., 2014). The following summer of 2014 was the rainiest over a 100-year record for Fairbanks (Euskirchen et al., 2020) and the summer of 2016 was the third wettest (Douglas et al., 2020). The warmest March on record was in 2019 with a mean monthly temperature of −2.4°C or 9.0°C above normal, which resulted in the earliest snowmelt on record. Our eddy covariance measurements now provide the opportunity to examine decadal responses to climate warming and extreme events as well as trends and interannual variability in C fluxes within this dynamic landscape. This task is particularly relevant since these extreme events are projected to continue in conjunction with warmer and wetter conditions (Bintanja & Andry, 2017; Overland, 2021; Walsh et al., 2018).

We examine our long-term data record with respect to the following questions: (1) Do we see trends in atmospheric C fluxes (CO_2 and CH_4) and associated micrometeorological variables, and if so, what are the probable drivers of these trends in the fluxes interannually and seasonally? (2) What is the magnitude of interannual variability and how may it be driven by climate trends and weather extremes? (3) How many years of data are needed to fully evaluate trends, and how might we expect trends to continue into the projected warmer future? and (4) What are the implications of our findings with respect to present and future carbon cycling as the landscape transitions under permafrost thaw?

2 | METHODS

2.1 | Site description

Our four eddy covariance measurement stations are located in a boreal peatland among the Tanana Flats lowland of Interior Alaska (64.70° N, −148.32° W, 100 m elevation; Figure 1a), ~30 km southeast of Fairbanks. The sites are associated with the Bonanza Creek Long Term Ecological Research Program (lter.uaf.edu; Figure 1a) and are part of the Alaska Peatland Experiment (APEX), which began in 2005 as an effort to understand water table conditions on carbon cycling

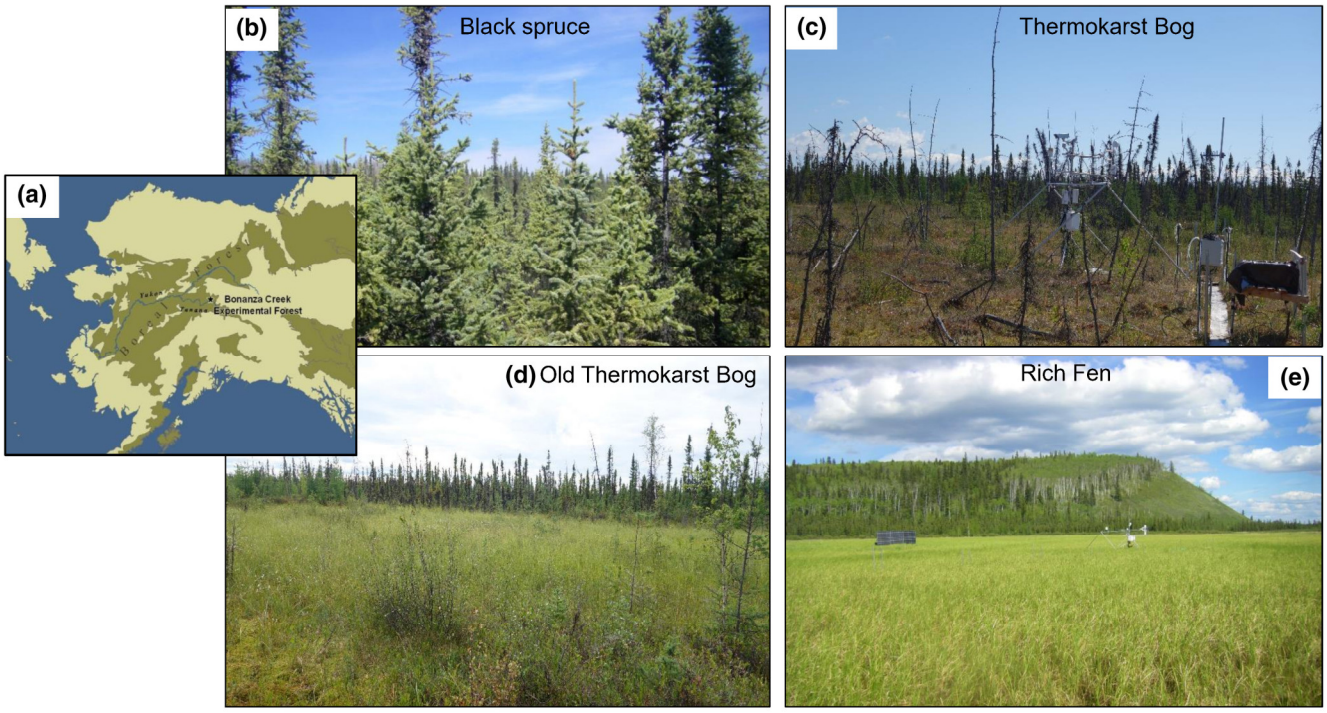

FIGURE 1 (a) Locations of the study sites in the Bonanza Creek Experimental forest of Interior Alaska and (b) photographs of the black spruce permafrost forest on a peat plateau, (c) the intermediate-aged thermokarst collapse scar bog, (d) the older thermokarst collapse scar bog, and (e) rich fen.

TABLE 1 Soil physical and chemical characteristics across the sites.

Site	Black spruce	Bog	Old bog	Rich fen
Ameriflux site name	US-BZS	US-BZB	US-BZO	US-BZF
Permafrost	Yes	Thawed	Thawed	No
No. of soil cores	12	2	2	3
Organic depth (cm)	64 ± 25	124 ± 9	89 ± 1	98 ± 6
Organic bulk density				
Mean ± SD	0.14 ± 0.11	0.07 ± 0.06	0.19 ± 0.14	0.17 ± 0.08
Range	(0.01–0.51)	(0.01–0.42)	(0.01–0.41)	(0.04–0.36)
% Soil C	38.1 ± 6.1	38.7 ± 4.9	39.3 ± 2.8[a]	39.4 ± 4.0
C storage ($kg\,m^{-2}$)	35.2 ± 22.0	41.9 ± 1.0	62.6 ± 30.7[a]	65.6 ± 0.8
Surface soil pH	5.6 ± 0.2	5.6 ± 0.1	4.8 ± 0.1	6.5 ± 0.2

[a]Carbon values derived from loss on ignition (LOI) measurements and the relationship between %C and LOI for other samples from this area.

at a rich fen (e.g., Chivers et al., 2009; Euskirchen et al., 2020; Kane et al., 2010; Olefeldt et al., 2017; Turetsky et al., 2008). This project has expanded to include thermokarst bogs and black spruce peat plateau sites (e.g., Euskirchen et al., 2014; McConnell et al., 2013; Neumann et al., 2019; Waldrop et al., 2021).

The sites are located about 500 m apart but vary in their presence and stability of permafrost and soil characteristics (Table 1). Sites include a black spruce peat plateau (Figure 1b) with cold permafrost soils, a collapse scar bog representing more recent permafrost thaw (Figure 1c), an older collapse scar bog representing less recent permafrost thaw (Figure 1d), and a rich fen lacking surface permafrost (Figure 1e).

The permafrost forest is dominated by mature black spruce trees (*Picea mariana*, ~100 years old), with a variable understory of shrubs, mosses, grasses, and lichens. The permafrost forest is on an intact peat plateau that rises ~130 cm from the surrounding landscape (Euskirchen et al., 2014). Collapse scar bogs are circular depressions that form over decades to 100s of years through thermokarst development. These sites contain active thaw margins with "drunken forest" and significant *Picea mariana* dieback. Thaw margins of the younger bog are dominated by indicators of recent permafrost thaw, including *Sphagnum riparium*. Radiocarbon dating of plant macrofossils at the boundary between the sylvic permafrost peat and post thaw collapse peat (marking the transition from lowland forest to

collapse scar feature) and Cs-137 dating of the peat profile suggest thermokarst initiated in the center of the younger collapse scar bog in the 1960s (Manies et al., 2021). The profile of the late successional collapse scar bog is detailed in Jones et al. (2012), with a chronology indicating the bog formed approximately 500 years ago when the permafrost thawed following fire. The rich fen lacks trees, is composed of grasses, sedges, and forbs, and formed from previous river channels with a groundwater regime that remains connected to the Tanana River. For brevity and ease of reading, throughout the manuscript we refer to the black spruce permafrost forest site as 'black spruce', the intermediate-aged collapse scar bog as 'bog', the late successional collapse scar bog as 'old bog' and the rich fen as 'fen'. We have also included the Ameriflux abbreviations for the sites in Table 1.

2.2 | Seasonality and climate of Interior Alaska

The region can be characterized by four distinct seasons. Winter, the 'cold season' (mid-October–March), has a continuous snowpack, little solar radiation, and a frozen ground surface. 'Spring' begins in early April with marked increases in day length and incoming solar radiation. Snowmelt occurs in mid- to late April and leaf out occurs by mid-May. By March, if air temperatures increase above 0°C, evergreens and bryophytes may begin to uptake CO_2 even with continued snow presence (Ueyama et al., 2006). The "growing season" lasts between mid-May and August. 'Fall' occurs between September and mid-October, with leaf senescence occurring by the third week of September and a snowpack forming by mid- to late October. For analysis in this paper, we consider the 'water year' as October 1–September 30. 'Winter' occurs between October 15–March 31, 'Spring' from April 1 to May 15, 'Summer' from May 16 to August 31, and 'Fall' from September 1 to October 15. These definitions are consistent with related studies of Euskirchen et al. (2014, 2020).

2.3 | Eddy covariance and biophysical measurements

Eddy covariance measurements of CO_2, latent, and sensible heat and associated meteorological measurements commenced in June 2010 in the black spruce permafrost forest, November 2010 in the bog, May 2011 in the fen, and June 2018 in the old bog. In April 2013, we initiated eddy covariance measurements of CH_4 at the bog, and in May 2014 eddy covariance CH_4 measurements began at the fen and spruce sites, with collection occurring from late April or early May through late September or early October each year. In May 2018, we moved the CH_4 instrument from the black spruce site to the old bog. CH_4 data were not collected year-round at the sites due to power limitations, but were typically collected between April–October, with exact periods differing from year-to-year (Table 2). Footprint analyses denote with 90% probability that the tower footprints are not overlapping and source areas are within the target ecosystem. Installation and data processing of these measurements were previously described in Euskirchen et al. (2014, 2020) but we provide an overview here.

Due to the remote site location, electrical power for instrumentation is provided by solar panels and batteries with the occasional use of a generator during December and January. Power systems consist of a 1400 W crystalline photovoltaic array charging a large (~5000 Ah) 12 V absorbent glass mat battery bank. Eddy covariance instrumentation for measuring fluxes of CO_2, CH_4, water, and energy is mounted in the center of the sites on a tripod at heights of 2 m in

TABLE 2 Dates of CH_4 data collection at each site from 2013 to 2022.

Year	Start and end dates			
	Bog	Fen	Black spruce	Old bog
2013	4/20–9/21	—	—	—
2014	4/13–10/30	4/16–10/31	—	—
2015	4/11–9/28	4/9–9/29	4/7–9/29	—
2016	4/1–11/2	5/4–10/31	3/31–10/16	—
2017	4/5–11/5	4/5–10/19	4/5–11/3	—
2018	4/15–11/5	4/6–9/29	—	4/6–11/4
2019	3/29–11/12	3/29–10/29	—	3/29–11/17
2020	4/18–11/2	4/17–10/26	—	4/15–10/31
2021	4/18–11/18	4/14–10/26	—	5/14–11/8
2022	3/23–11/29	3/23–11/5	—	3/23–11/2
Common period	4/20–9/21	5/4–9/29	4/7–9/29	5/14–10/31
Common period bog and fen: 5/4–9/21 from 2014 to 2022				
Common period bog, fen, and old bog: 5/14–9/21 from 2018 to 2022				

Note: 'Common period' refers to the dates when data collection occurred across all years for the site specified in the column or as specified across a group of sites, 'bog and fen' and 'bog, fen, and old bog'.

the fen and 3 m in the bogs. Instrumentation was mounted at 5 m on a triangular tower at the black spruce site.

Instrumentation consists of a three-dimensional sonic anemometer (CSAT-3; Campbell Scientific Instruments, Logan, UT, USA) and an open-path infrared gas analyzer (LI-7500 IRGA; LI-COR, Lincoln, NE, USA) at the permafrost forest and old bog, and an EC-150 (Campbell Scientific Instruments, Logan, UT, USA), at the fen and bog for measurements of CO_2, latent, and sensible heat fluxes. Measurements of CH_4 fluxes are performed with a fast-response open-path methane analyzer (LI-7700; LI-COR, Lincoln, NE, USA), which uses a LI-7550 interface unit to control mirror heating and cleaning cycles and to route the high-frequency data to the datalogger. All instrumentation is connected to a digital datalogging system to log data at 10 Hz intervals.

Basic microclimatic data are also collected, including photosynthetically active radiation (PAR; 2 m above the ground; LI190SB, LI-COR), air temperature (T_a) and relative humidity (RH; 2 m above the ground; HMP45C, Vaisala, Helsinki, Finland), soil water content (water content reflectometers at 2 and 6 cm depth, CS616, Campbell Scientific Instruments), soil heat flux (two replicates at 5 cm below the surface, HFP01-SC, Hukseflux, Delft, Netherlands), precipitation as rain was measured with a tipping bucket (2 m above the ground; TE525MM, Texas Electronics, Dallas, TX, USA), net radiation (2 m above the ground; NR-LITE; Kipp and Zonen, Delft, Netherlands), snow depth (2 m above the ground; SR50A, Campbell Scientific Instruments), albedo (2 m above the ground; albedometer CMA6, Kipp and Zonen), soil temperature (T_s at 2 and 6 cm depth; TCAV; averaging soil thermocouple probe; Campbell Scientific Instruments), and barometric pressure (PB105, Vaisala). Snow water equivalent (SWE) data are collected with a precipitation weighing assembly (ETI NOAH III; Fort Collins, CO, USA; Van Cleve et al., 2018). These variables are measured at 1 s intervals and stored on the datalogging systems. Both the processed eddy covariance and microclimatic data are averaged for 30 min periods. Photographic images are collected once a day with a StarDot Netcam (StarDot Technologies, Buena Park, CA, USA). Water table levels at the fen, bog, and old bog are measured using a pressure transducer (Campbell Scientific, Logan, UT) installed at the bottom of a 5 cm diameter, 1 m long PVC well.

Depths of the seasonally frozen and thawed active layer (top of near-surface permafrost) have been measured at six locations at the APEX complex since 2008 (Manies et al., 2021, 2023). A thin (1-cm diameter) rod is pushed into the soil until refusal and distance from the moss/lichen surface to this depth is measured. Active layer thickness (ALT) measurements are repeated between August and October and are located within six sites in the permafrost plateau area between the black spruce and bog flux towers. Data are plotted by each location over time with a linear regression model fit to the data to examine trends in active layer by area and year. We examine the relationship between ALT for a given year and precipitation, looking separately between total and monthly summer rain and total SWE from the water year.

2.4 | Data processing

2.4.1 | Eddy covariance data

Eddy covariance data processing and post-processing are performed as described in Euskirchen et al. (2014, 2020) and are available through the Ameriflux database (Euskirchen, 2022a, 2022b, 2022c, 2022d). A CO_2 signal strength diagnostic, which represents optical impedance by precipitation or aerial contaminants, is provided by the infrared gas analyzers. This diagnostic is used as a quality assurance/quality control variable for both flux and radiation data. The "WPL" terms are applied during post-processing to the CO_2 and latent heat fluxes to account for changes in mass flow caused by changes in air density (Webb et al., 1980). Corrections are applied to account for frequency attenuation of the eddy covariance fluxes (Massman, 2000, 2001). For the consideration of nocturnal CO_2 advection, we calculate a storage term and then performed a friction velocity (u^*) correction for calm periods, when u^* was less than 0.1 m s^{-1}, which was determined through applying the u^* analysis in REddyProc (Wutzler et al., 2018).

Data gaps occur because of instrument malfunction, power outages, instrument calibration, or occasional generator use in December and January. Shorter gaps (≤1 day) in eddy covariance data are usually related to instrument errors during precipitation. Longer gaps (1–2 weeks) occur due to power outages and instrument shutdown during cold temperatures. We did not gap-fill the 9 months (March–December) in 2014 and for three and a half months in 2022 (mid-September–December) when data were lost from the black spruce site due to malfunction with the gas analyzer. For data gaps of approximately 1–6 days, we gap fill by calculating the mean diurnal variation where a missing observation is replaced by the mean for that time period (half hour) based on adjacent days (Falge et al., 2001). Marginal distribution sampling is used to gap-fill larger data gaps of 1–2 weeks (Reichstein et al., 2005). We use the ReddyProc software for gap-filling (Wutzler et al., 2018). Over the entire study period, the percentage of data collected was near 95% from March to October, excluding the two periods from the black spruce when the gas analyzer malfunctioned. Between November and February data collection was ~75%. Data coverage during the entire period was approximately 85% after accounting for data loss from power outages, instrument malfunction, precipitation, and u^* filtering.

The error in eddy covariance measurements due to u^* uncertainty, data gaps, gap-filling techniques, and inherent random measurement error were quantified using bootstrapping to estimate the error (a 95% confidence interval) about the total NEE, GPP, ER, and CH_4 estimates (Papale et al., 2006; Wutzler et al., 2018). Given that the u^* uncertainty can be significant, this is estimated separately in ReddyProc. This estimated u^* uncertainty is then added to the bootstrapped error based on the remaining sources of uncertainty.

2.4.2 | Partitioning net ecosystem exchange into gross primary productivity and ecosystem respiration

While we do not directly measure GPP and ER, NEE based on eddy covariance data can be partitioned into these counterparts to provide an approximation of ER and GPP and therefore a general understanding of photosynthetic versus respiratory controls over NEE. This partitioning is calculated by employing the algorithm described in Reichstein et al. (2005), using the ReddyProc software (Papale et al., 2006; Reichstein et al., 2005; Wutzler et al., 2018). The partitioning is performed based on nighttime temperature, where 'nighttime' is defined as PAR $<50\,\mu mol\,m^{-2}\,s^{-1}$. The algorithm fits a respiration model to the measured nighttime NEE data and then extrapolates the optimized model to the daytime using temperature observations during the day. An Arrhenius-type model after Lloyd and Taylor (1994) is used to derive and extrapolate the temperature dependence of ER. The difference between modeled ER and measured NEE provides the GPP estimate. For consistency with NEE, greater negative values of GPP correspond to greater productivity.

2.4.3 | Growing degree days and determination of snow melt and snow return

We calculate cumulative growing degree days (GDD) based on mean daily air temperature (T_a) for both the measurement sites and the 30 year mean, as GDD = Σ max (0, $T_i - 0$), where T_i is the mean daily T_a and the base is 0°C. We use 0°C as the base temperature since, as noted above, both the black spruce trees and bryophytes may photosynthesize at temperatures above freezing even with continued snow presence.

As in Euskirchen et al. (2020), we determine the date of snow return in the autumn by observing at which point albedo remained above 0.3 (30% radiation reflected) in conjunction with mean daily air temperatures at or below freezing, and snow presence as measured with the snow depth sensor and snow bucket. Timing of snow melt is determined by albedo measurements below 0.3, mean daily air temperatures above freezing, and an absence of snow measured by the snow depth sensor and the snow bucket. Our dates are also cross-checked with visual webcam images.

2.4.4 | Methane emissions and global warming potential

While we do not measure CH_4 emissions year-round there were some years when CH_4 measurements begin prior to snowmelt and when soil temperatures (~2 cm depth) remain below 0°C (Table 2). Based on these cold season periods when soils are frozen (March–early April) and CH_4 data are available, we provide a rough estimate of cold season CH_4 emissions for the fen, bog, and old bog. We also separately examine emissions from October to early November in years when data are available to gain a better understanding of fall and early winter emissions, prior to soil freeze. We compare these mean daily estimates of cold season and fall emissions to those between May–September to identify seasonal differences.

To provide an overall estimate of C emissions from our study sites, the CH_4 data are converted to CO_2 equivalents (CO_2 e) by multiplying the CH_4 flux by the 100-year global warming potential (GWP) of methane, estimated at 28 (Myhre et al., 2013). We use the conventional GWP metric over other recently discussed metrics, such as the sustained GWP (SGWP), which is also subject to shortcomings (Neubauer & Megonigal, 2015). The SGWP would result in an estimated 38% higher CO_2 e values, estimated at 45 over a 100-year timescale compared to 28 for GWP, and thereby the GWP provides a more conservative estimate.

2.5 | Trend analysis and significant difference tests

We assessed trends in metrics related to biophysical variables and fluxes collected at our sites. This included time series of day of snow return and snow melt, snow season duration snow season, total snow water equivalent (SWE) over the water year (October 1–September 30), total precipitation (rain plus SWE), soil water content, and soil temperature. For fluxes, we assessed trends in annual NEE, GPP, ER, and winter ER (or, equivalently, winter NEE). We also assessed trends in CH_4 during periods when data were collected.

This trend analysis was similar to that conducted in Euskirchen et al. (2017). We first tested for autocorrelation in the time series using autocorrelation and partial autocorrelation functions (acf, pacf in R software version 3.2.3). Since we did not detect autocorrelation or partial autocorrelation in our variables we applied the nonparametric Mann-Kendall test for trend at the 5% significance level on the data. We also computed the magnitude of the trend (a trendline with a slope) based on the Theil-Sen approach (Sen, 1968).

To examine significant differences across sites for annual means in cumulative NEE, GPP and ER, we implemented the agricolae package in R to perform an ANOVA and initially test for significant differences across sites, followed by a Tukey's honestly significant difference test to determine which sites were significantly different. To test for significant differences in seasonal CH_4 emissions within a given site, we performed a Games-Howell test using the rstatix package in R.

2.6 | Empirical models

To better understand environmental factors influencing annual values of NEE, GPP, ER, and winter ER (based on winter ER calculated over the water year) and CH_4 emissions with the decadal time series (i.e., excluding the old bog site) we developed empirical models of these fluxes versus environmental variables based on data summarized at both the monthly and annual time scale. These variables include total annual rainfall, total rain and snow over the water year, mean summer (June 1–August 31), winter (October 15–March 30),

fall (September 1–October 14), and spring (April 1–May 31) soil temperatures, growing degree days, total evapotranspiration, mean summer soil water content, day of snowmelt, day of snow return, duration of the snow season, air temperature, vapor pressure deficit, atmospheric pressure, and water table depth based on best fit multiple regression equations. For the models based on monthly data, we also examined if total precipitation (rain + SWE) and soil temperature from the previous month were significant predicators of cumulative fluxes for the current month. For models based on annual data we examined one variable at a time, given the known correlations between temperature and precipitation and the potential to having too few degrees of freedom. We were also interested in determining if simple models could be useful for predicting annual fluxes. We tested various models including linear, exponential, and parabolic based on the environmental variables. Best fit was determined using Akaike's information criteria compared across models for a given season and ecosystem. If Akaike's information criteria were the same for two models both models are presented.

We performed additional analysis at the fen site to ensure the seasonal analysis of early (May–June) and mid-late (July–September) dry (water table depth ≤0 cm) and wet (water table depth >0 cm) period controls on carbon fluxes remained consistent with the findings of Euskirchen et al. (2020), which included only the data from the years 2011–2018. That is, we added 4 years of data from 2019 to 2022 to the analysis. Specifically, we examined how early season wet periods, coincident with runoff from snowmelt, and later season wet periods, coincident with inundation from rainfall, were associated with CO_2 uptake and release and CH_4 emissions.

Moisture status of the fen was classified from May to September from 2011 to 2022 when water table depths were available. These four classes included: (1) early season dry: days in May and June when the water table is below the surface, (2) early season wet/inundated: days in May and June when the water table is above the surface, (3) mid-late season dry: days in July, August, or September when the water table is below the surface, and (4) mid-late season wet/inundated: days in July, August, or September when the water table is above the surface.

We evaluated the influence of moisture status classification on fluxes by calculating adjusted means with an analysis of covariance model (ANCOVA), including mean daily soil temperature (T_s, 7.5 cm depth) for each of the cumulative daily fluxes. NEE, ER, GPP and CH_4:

$$\text{Flux} = \text{Moisture Status} \times T_s \times \left(T_s \times \text{Moisture Status}\right). \quad (1)$$

The above analysis indicated the slopes for the interaction term, $T_s \times$ Moisture Status, were unequal ($p < .0001$) for all fluxes, thereby not meeting the ANCOVA assumption of equal slopes. We thus applied an unequal slopes model (Neter et al., 1996) of the form:

$$\text{Flux} = \text{Moisture Status} \times \left(T_s \times \text{Moisture Status}\right). \quad (2)$$

We used the 'proc glm' procedure in SAS for Equation (1) and the 'proc mixed' procedure in SAS for Equation (2) (version 9.4, SAS Institute, Cary, NC).

2.7 | Regional scaling

We provide an approximation of C emissions in boreal lowlands for the years 2011–2022 based on the NEE and CH_4 data. We provide separate estimates for both the Tanana Flats (2640 km^2) and all of the boreal lowlands in Alaska, including the Tanana Flats. Lowlands comprise approximately 42% of the 574,000 km^2 boreal land area in Alaska (Douglas et al., 2014). Of the Tanana Flats and the entire lowland area, roughly 24% is classified black spruce, 40% as low fens, 7% as thermokarst collapse scar bogs, and the remainder is categorized as lowland birch or mixed forest and low scrub vegetation (Douglas et al., 2014; Jorgenson et al., 2001). That is, the vegetation within the footprints of our eddy covariance towers is represents ~71% of the Tanana Flats and the overall boreal lowland vegetation in Alaska. For the fens, this equates to an area of 1056 km^2 for the Tanana Flats and 96,432 km^2 for all boreal lowlands and for the collapse scar bogs, this equates to 185 km^2 for the Tanana Flats and 16,876 km^2 for the lowlands. For the black spruce, this equates to an area of 634 km^2 for the Tanana Flats and 57,859 km^2 for the lowlands. We scale our estimates to the Tanana Flats and boreal lowland area by considering the mean annual fluxes of NEE and CH_4 (Figure 7) for the rich fen, bog, and black spruce forest and using our mean annual bootstrapped error estimates (Table S3) of these fluxes to provide upper and lower bounds on our measurement annual means. We also examine scenarios with variation in the percent of the landscape that is fen (15%–50%), bog (10%–15%) and black spruce (50%). We chose these scenarios to demonstrate how increases in permafrost degradation and the associated vegetation shifts may influence landscape-level C emissions. For example, increasing the prevalence of one vegetation type with low C emissions (e.g., black spruce, which is associated with more stable permafrost) may result in much lower landscape-level emissions, while decreasing the prevalence of a vegetation type with higher C emissions (e.g., fens and collapse scar bogs, associated with permafrost thaw) may result in much higher landscape-level C emissions.

3 | RESULTS

3.1 | Trends in meteorological and biophysical variables

We observed increasing precipitation as both rain and snow water equivalent from 2005 to 2022. The historical mean total rainfall amount for this area is ~160 mm and the historical SWE is ~90 mm (1990–2004; NOAA, 2021). Each year beginning in 2014 received above average rainfall with a mean of 220 mm each water year 2005–2022 (Figure 2a). Precipitation as snow, with mean of 126 mm SWE each water year from 2005 to 2022, accounted for a mean of 37% of the total precipitation as both rain and snow.

Even though there was a significant increase in SWE from 2005 to 2022 (Figure 2b), this trend was coupled with a shorter

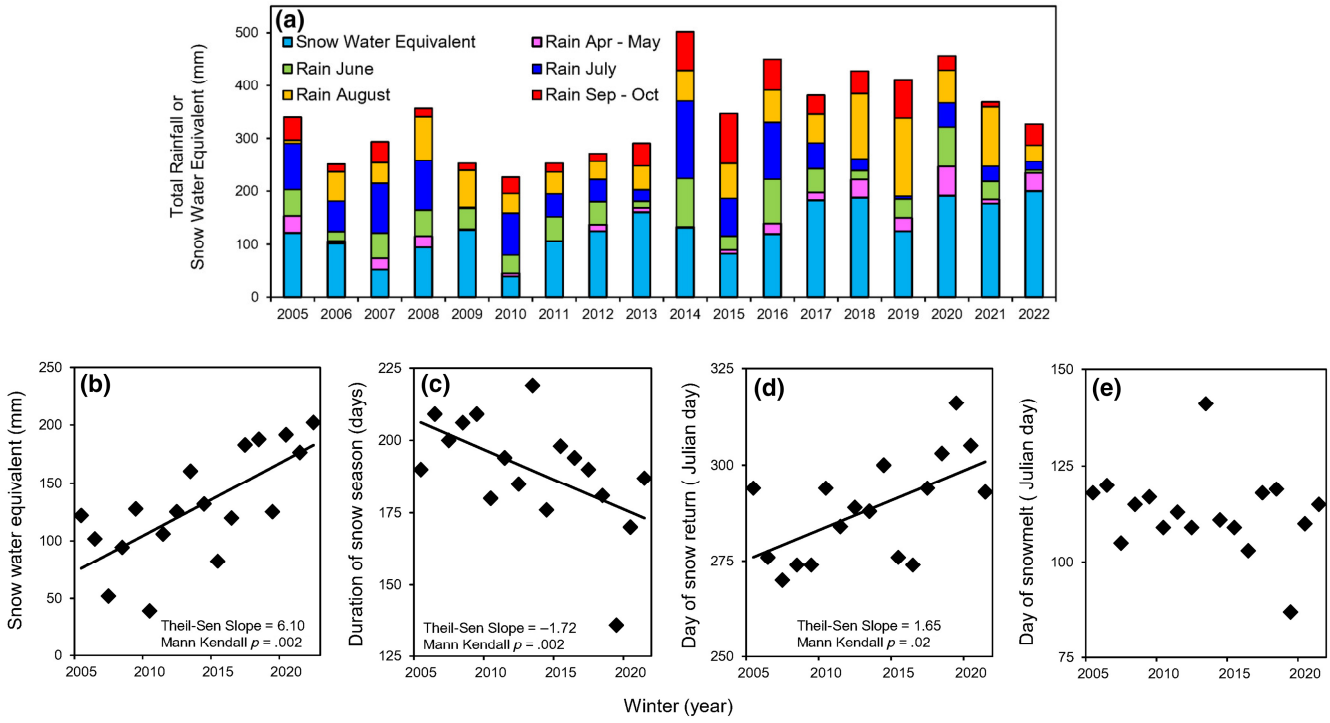

FIGURE 2 In (a), total snow water equivalent (SWE) and rain (mm) for each water year October 1, 2004–September 30, 2022, and between October 1–April 30 for 2022 for SWE. Trends in SWE (b), the duration of the snow season (c), day of snow return (d), and day of snowmelt (e). The slope of the line is based on the Theil-Sen estimate, and the significance is assessed using a Mann–Kendall test, as described in Section 2. There is no trend line shown for the day of snowmelt (e) since there was not a statistically significant trend.

snow season duration (Figure 2c), which was primarily due to a later return of snow in the fall (Figure 2d). There was not a statistically significant trend in the day of snowmelt onset although the earliest snowmelt on record for Fairbanks occurred in March 2020, resulting in the shortest snow season recorded during our measurements (Figure 2e).

Despite above-average rainfall, the water table depth measured with the pressure transducers at the collapse scar bogs typically remained below the surface because the peat layer floats on the surface (Figure 3a; Neumann et al., 2019). The rich fen remained flooded (water table depth >60 cm above the surface) in 2014, 2017, 2018 and 2020 (Figure 3b).

Winter soil temperatures (7.5 cm depth) increased significantly in the black spruce and rich fen (Figure 4a) as did fall soil temperatures in the bog (Figure 4b). Surface soil water content (5 cm depth) increased significantly from 2011 to 2022 in the bog (Figure 4c). The rich fen soil water content data were not reliable due to the flooding at the site.

Active layer thickness (ALT) nearly doubled with average depth to permafrost less than 40 cm in 2008 and 2009 and between 57–73 cm for the years of 2015–2022 (Figure 5; Tables S1 and S2). In addition, the variability of active layer thicknesses increased 3–4 times between these two time periods. Although there was a positive relationship between ALT and precipitation, this was not significant ($R^2 = 0.2$, $p > .05$).

3.2 | CO_2 fluxes: Net ecosystem exchange, gross primary productivity, and ecosystem respiration

All the sites were neutral to slight sources of CO_2, with means ranging from 13 ± 31 g C m^{-2} year^{-1} at the black spruce site, 23 ± 23 g C m^{-2} year^{-1} at the bog and 50 ± 17 g C m^{-2} year^{-1} at the rich fen which was a significantly greater CO_2 source than the black spruce and bog (with ± error based on the bootstrapping methodology described in Section 2.4.1 and shown in Table S3; Figure 6a; Figures S1 and S2, with u^* uncertainty representing on average 25% of total uncertainty). In the black spruce and rich fen, interannual variability in NEE (represented as the standard deviation of the mean total annual NEE over the period of record) was higher (±102 and 113 g C m^{-2} year^{-1}, respectively), than that of the collapse scar bog (±58 g C m^{-2} year^{-1}).

Both GPP and ER were significantly larger at the black spruce site compared to the bog and fen (Figure 6b,c). Winter ER was greatest at the fen, and this was significantly different from that of the bog, but not that of the black spruce (Figure 6d). Winter ER accounted for ~16% of total ER at the bog and black spruce sites and 24% at the fen. GPP and ER were greatest between late June and July, with GPP falling to zero or nearly zero during the period of snow-covered ground from October to mid-April (Figure S3). There were no statistically significant trends over time in the annual fluxes of NEE, GPP, and ER.

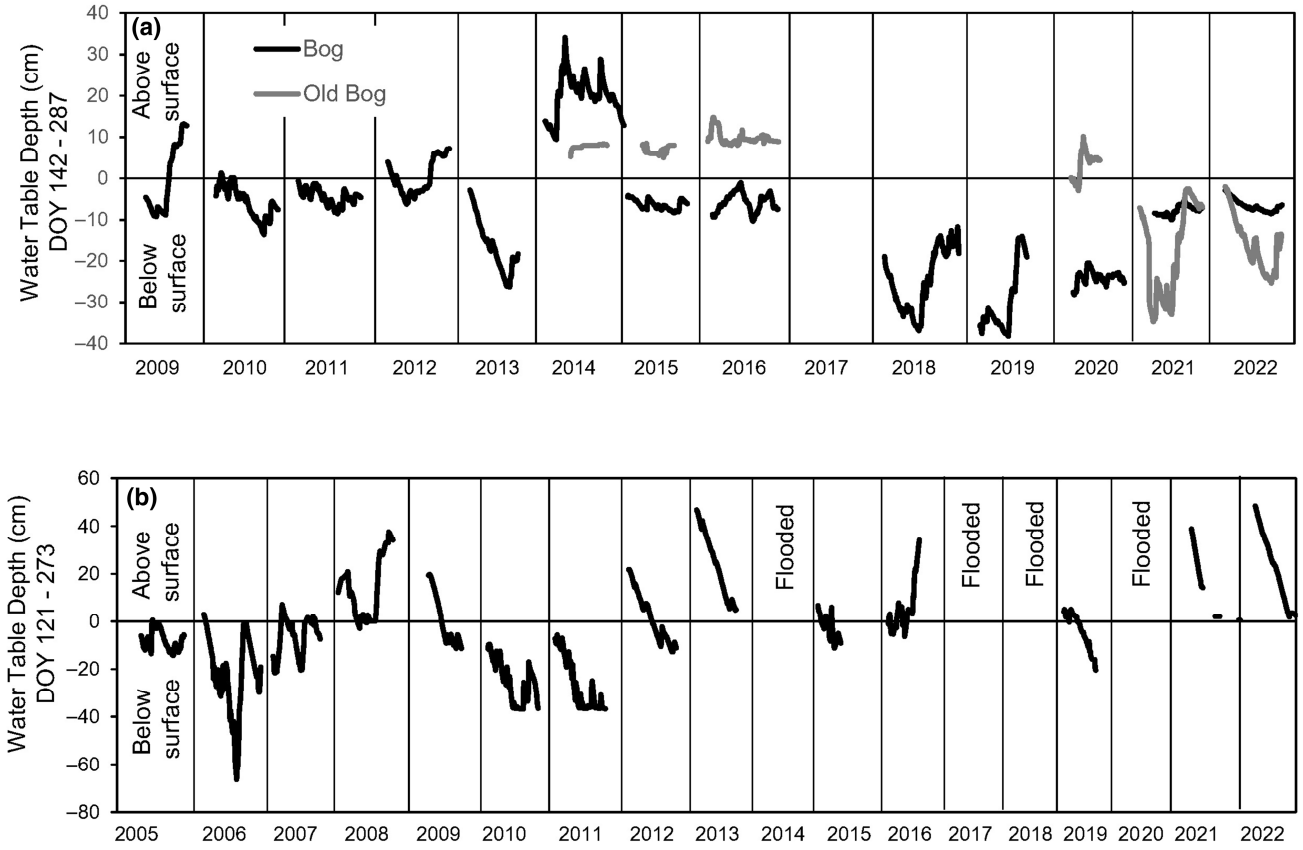

FIGURE 3 Water table depth (cm) from May to September in the bog from 2009 to 2022 and old bog from 2020 to 2022 (a) and fen from 2005 to 2022 (b). In years marked as flooded, water table depth exceeded 60 cm above the surface and was not measured.

Comparing across the bog, old bog, fen, and black spruce sites for the years when annual data were available for all four sites (2019–2021; Figure 6e–h) mean annual NEE for the bog ($46 \pm 13\,g\,C\,m^{-2}$) and old bog ($47 \pm 24\,g\,C\,m^{-2}$) was essentially the same, with the most uptake occurring at the black spruce site during 2019–2021 ($-82 \pm 29\,g\,C\,m^{-2}$; Figure 6e, with ± error based on the bootstrapping methodology described in Section 2.4.1 and shown in Table S3). There were year-to-year differences between the bog and old bog. For example, in 2019, the bog was a source of CO_2 with a total annual NEE of $18 \pm 11\,g\,C\,m^{-2}$ while the old bog was a sink of CO_2 with a total annual NEE of $-12 \pm 17\,g\,C\,m^{-2}$ and in 2021 when the old bog was a larger source of CO_2 ($131 \pm 15\,g\,C\,m^{-2}$) compared to the bog ($82 \pm 11\,g\,C\,m^{-2}$; Figure S1).

3.3 | Empirical models of NEE, GPP, and ER

At the black spruce, bog, and fen, total (cumulative) NEE, GPP, ER, and winter ER fluxes were related to precipitation amounts (total annual rain and total snowfall in terms snow water equivalent) and timing of snowfall in the fall (day of snow return with onset of albedo above 0.3, as described above; Table 3). At the fen, total annual NEE was parabolically related to GDDs, and linearly increased/decreased with total annual rainfall. Winter ER at each site was exponentially related to winter soil temperature. Larger amounts of total rainfall (April–October rainfall) and snow in terms of SWE also increased winter ER.

At the fen, based on Equations (1) and (2), CO_2 fluxes from May to September were related to inundation status and soil temperature (Table 4; Figure S4). Both NEE and GPP showed the least ecosystem C uptake during early season wet periods coincident with inundation from snow and wet conditions prior to freeze in the late fall ($-0.2\,g\,C\,m^{-2}\,day^{-1}$ for NEE and $-3.1\,g\,C\,m^{-2}\,day^{-1}$ for GPP during the early season inundation and $-0.5\,g\,C\,m^{-2}\,day^{-1}$ for NEE and $-3.7\,g\,C\,m^{-2}\,day^{-1}$ for GPP during late season wet conditions, considering adjusted means controlling for soil temperature; Figure S4a,b). The most net C uptake occurred during mid-late season dry periods (NEE of $-1.3\,g\,C\,m^{-2}\,day^{-1}$). The greatest amount of ER occurred during early season dry conditions ($3.2\,g\,C\,m^{-2}\,day^{-1}$; Figure S4c).

3.4 | CH_4 fluxes across sites

We compared mean CH_4 emissions between the fen and bog for the years 2014–2022 during a consistent measurement period from May 4 to September 21 (Table 2; Figure 7a). Emissions varied between the two sites and were ~20% greater from the fen (Figure 7a). We performed a similar comparison between the fen, bog, and old bog for the years 2018–2022 and the period from May 14 to September 21 when data were collected across the three sites. There were no

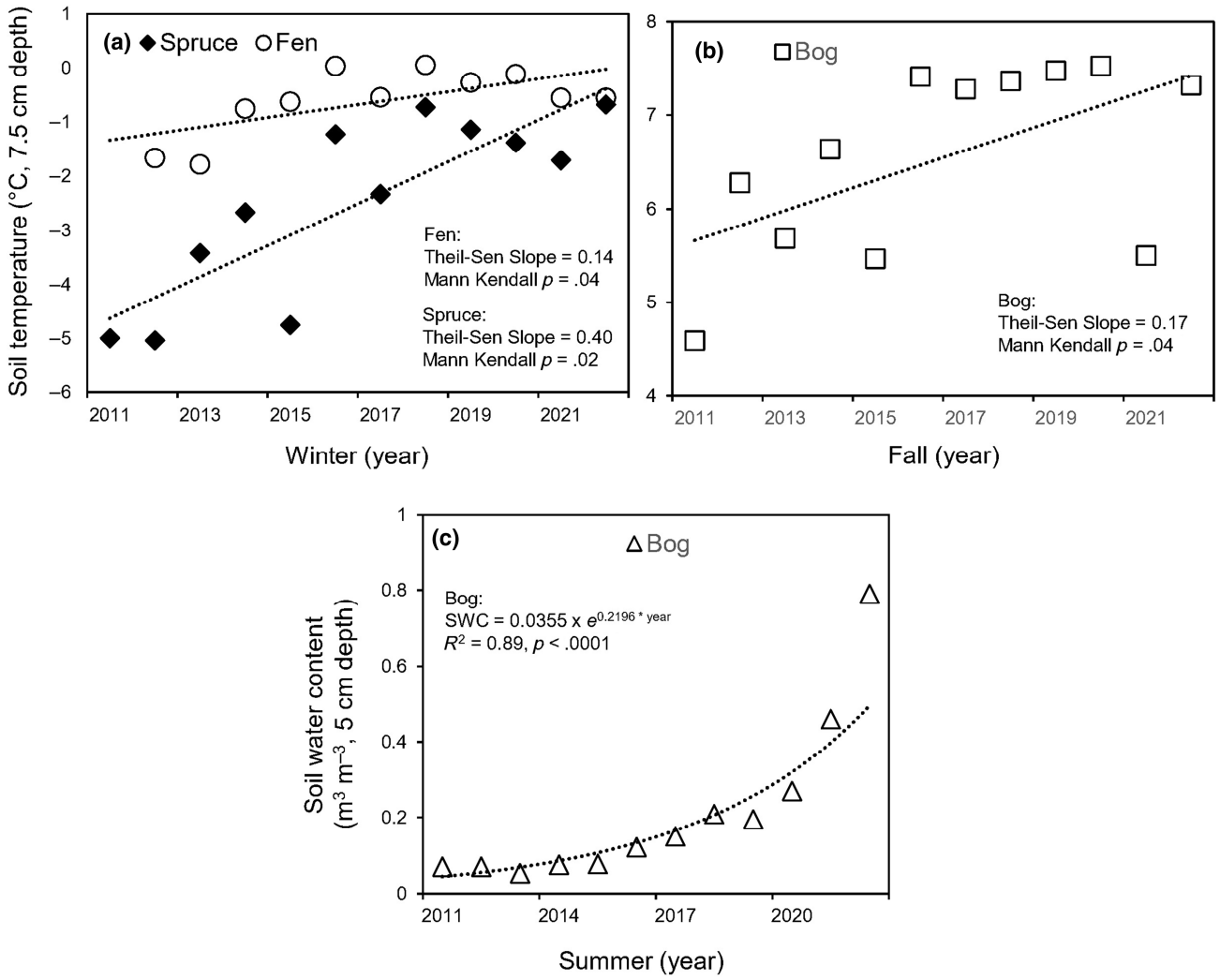

FIGURE 4 Trends in soil temperature (7.5 cm depth) during the winter from 2011 to 2022 for the black spruce and fen sites (a) and during the fall in the bog (b). In (c), the trend in soil water content (5 cm depth) during the summer from 2011 to 2022 in the bog. The slope of the line is based on the Theil-Sen estimate, and the significance is assessed using a Mann–Kendall test, as described in Section 2.

statistically significant differences between the sites, although emissions again remained greater (by ~17%) from the fen (Figure 7b).

At all three sites, emissions of CH_4 were highest in the warm season from May to September, intermediate in the fall between October and November, and lowest in periods in early April, corresponding to the cold season when surface soils remained frozen (Figure 7c). Our estimate of cold season CH_4 emissions for the fen was $1.3 \pm 4.6\,mg\,CH_4\,day^{-1}$ based on periods in late March and early April when the CH_4 measurements occurred and soil surface temperatures remained below freezing (Figure 7c). Assuming relatively constant emissions during cold periods and multiplying $1.3\,mg\,CH_4\,day^{-1}$ by the number of cold season days (~150) adds approximately $0.193\,g\,CH_4\,year^{-1}$ of CH_4 emissions from the fen, or ~2% of the mean annual emissions measured each year from May 14 to September 21, 2014–2022 (Figure 7b). At the bog, cold season CH_4 emissions in early April were $0.007.6 \pm 0.008.7\,g\,CH_4\,day^{-1}$ (Figure 7c), increasing estimates of mean annual emissions by $1.1\,g\,CH_4\,year^{-1}$ or ~10% of the mean annual emissions measured each year from May 14 to September 21, 2014–2022 (Figure 7b). For the old bog, our estimate of cold season emissions was $22.3 \pm 8.5\,mg\,CH_4\,day^{-1}$, corresponding to $3.2\,g\,CH_4\,year^{-1}$ of CH_4 emissions, or 32% of the mean annual emissions measured between May 14–September 21 (Figure 7b).

Emissions of CH_4 from the bog from April 20 to September 21, 2013 to 2021 were logarithmically related to summer soil water content (based on the mean summer SWC at 2 and 6 cm depths). At the fen, CH_4 emissions decreased exponentially as net growing season CO_2 uptake at the fen decreased (Figure 7e). Based on Equations (1) and (2), CH_4 emissions at the fen were greatest during both early season wet and mid- to late season dry conditions (~$0.08\,g\,CH_4\,m^{-2}\,day^{-1}$; Table 4; Figure S4d) and lowest during early season dry conditions (~$0.05\,g\,CH_4\,m^{-2}\,day^{-1}$).

3.5 | Cumulative carbon emissions in CO_2 e

Considering all available measurements of CH_4 (beginning between 2013 and 2014 at the bog and fen, respectively, and the old bog in 2018; Table 2), converting them to CO_2 equivalents

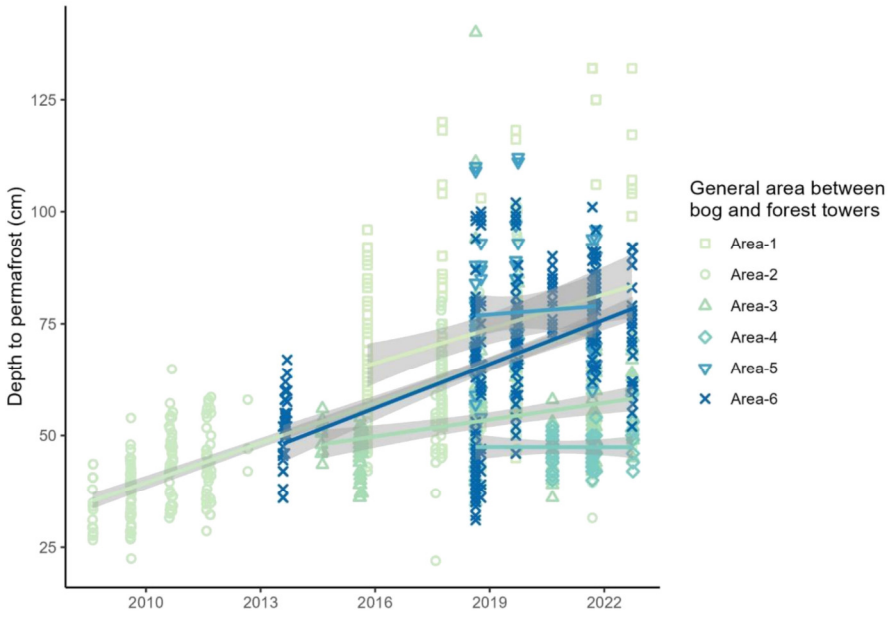

FIGURE 5 Depth of permafrost (cm) over time at six different sites in the permafrost plateau area of the APEX site.

(CO_2 e; Section 2), and adding them to measured NEE allowed us to consider total emissions of CO_2 e based on our measurements (Figure 8). The emissions were largest at the fen, where CH_4 emissions added an additional ~3550 $g\,CO_2\,e\,m^{-2}$ (CH_4+CO_2: 5263 $g\,CO_2\,e\,m^{-2}$; CO_2 only: 1716 $g\,CO_2\,e\,m^{-2}$; Figure 8c). Emissions at the bog were slightly less than the fen, where CH_4 emissions added an additional ~3176 $g\,CO_2\,e\,m^{-2}$ (CH_4+CO_2: 4210 $g\,CO_2\,e\,m^{-2}$; CO_2 only: 1034 $g\,CO_2\,e\,m^{-2}$; Figure 8c). Measurements of CH_4 in the black spruce site were low (Figure 8b), adding an additional 77 $g\,CO_2\,e\,m^{-2}$ to the measurements of NEE between the years 2015–2017 (Figure 7c). At the old bog, CH_4 emissions added an additional ~1657 $g\,CO_2\,e\,m^{-2}$ (CH_4+CO_2: 2163 $g\,CO_2\,e\,m^{-2}$; CO2 only: 507 $g\,CO_2\,e\,m^{-2}$; Figure 8d).

3.6 | Regional scaling

By scaling our continuous measurements of CO_2 and CH_4 from 2011 to 2022 (Figure 9) to the vegetation types by the boreal lowland area in Alaska (574,000 km^2), we estimate a cumulative release of 0.30–0.40 Pg C from the represented boreal lowlands during this time, considering fen, bog, and black spruce land cover comprises 40%, 7%, and 24% of the landscape, respectively, with the upper and lower bounds based on bootstrapping (Figure 9). In this estimate, the release of C from boreal fens dominates the carbon signal (0.29–0.34 Pg C). If we consider an increase in fen area to 45% coverage and thermokarst collapse scar bog to 10% coverage, estimated landscape emissions rise to 0.35–0.47 Pg C. An additional increase to fen area with 50% coverage and thermokarst bog area with 15% coverage results in 0.41–0.55 Pg C estimated emissions. Considering a different landscape scenario where black spruce forest dominates 50% of the lowland landscape and fens shrink to 15% while the bogs remain at 7%, emissions drop to 0.09–0.21 Pg from 2011 to 2022. Taking into account only the Tanana Flats region (2640 km^2) of this boreal lowland landscape (Figure 9), these estimates are smaller. We estimate cumulative release of 1.6 9×10^{-3} Pg C in the lower bound scenario with black spruce comprising 50% of the landscape to 6.0×10^{-3} Pg C in the upper bound scenario where fens comprise 50% of the landscape.

4 | DISCUSSION

4.1 | Source versus sink strength of C across the circum-boreal region

Previous studies indicate that, excluding anthropogenic fossil fuel emissions, the boreal region is currently a net C sink, although this sink strength may change in the future towards either a greater net release or uptake of C. For example, climate-related disturbances such as wildfire and permafrost thaw (e.g., Bradshaw & Warkentin, 2015; Helbig, Chasmer, Desai, et al., 2017; Helbig, Chasmer, Kljun, et al., 2017; Manies et al., 2021; Zhuang et al., 2020) as well as human impacts from land clearing and road construction, may result in greater C release. Greater uptake may be due to increases in GPP that are not fully offset by increases in ER, particularly in boreal upland forests (Liu et al., 2022) and drought that may result in reductions in CH_4 emissions (Heiskanen et al., 2021). Bradshaw and Warkentin (2015) applied an inventory approach to estimate C storage and flux in the circum-boreal region and determined it was a net sink of 364–1716 Pg C but the region may be transitioning to a net C source due to warming and both natural and anthropogenic disturbances. Zhuang et al. (2020) applied a process-based model to simulate North American peatland C storage over the last 12,000 years and found that these peatlands accumulated 85–174 Pg C over the study period, but that peat decomposition and permafrost degradation complicate future predictions of the sink strength (Jones et al., 2023). Two

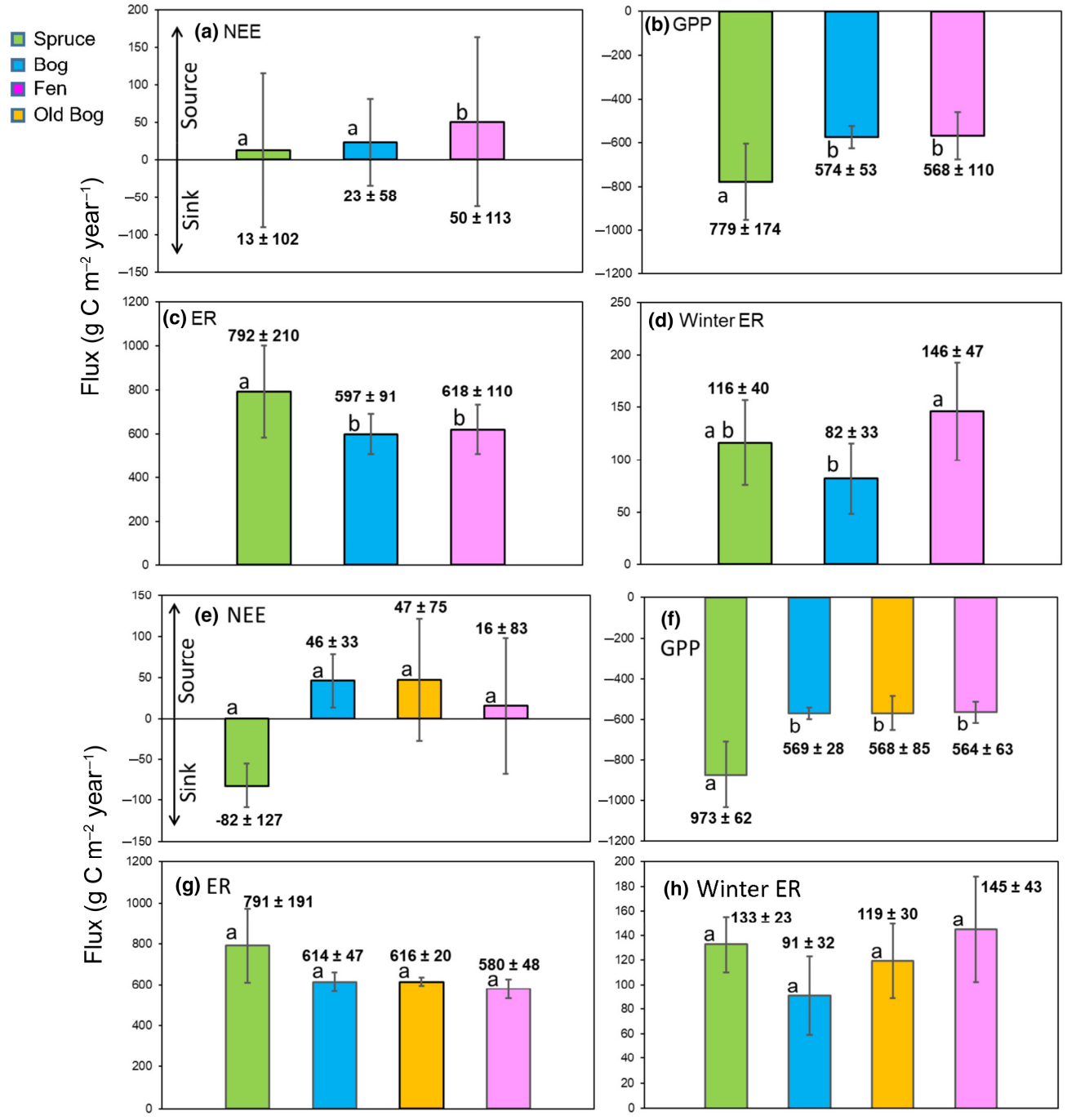

FIGURE 6 Mean (standard deviation) annual net ecosystem exchange (NEE, a), gross primary productivity (GPP, b), ecosystem respiration (ER, c), and winter ecosystem respiration (winter ER, d) from 2011 to 2022 in the black spruce, bog, and rich fen. Panels (e–h) are similar, except these include data from 2019 to 2022 in the black spruce, bog, old bog, and rich fen. Different letters indicate significant differences between sites for a given flux based on a Tukey HSD test.

studies conducted at the pan-Arctic scale indicate, based on CO_2 alone, the boreal region remains a net sink of CO_2 for the years 1990–2015 with much of this sink strength derived from the boreal uplands, particularly those in the Eurasian boreal region, and Siberia in particular (Virkkala et al., 2021; Watts et al., 2023). Considering only evergreen boreal forests, recent work finds a net sink of 0.4 Pg C year^{-1} between 1981–2018, but there is no trend toward increasing in CO_2 uptake as increases in GPP are compensated for by losses due to ER, with large interannual variability (Pulliainen et al., 2022).

However, when both CO_2 and CH_4 are included in calculations of greenhouse gas forcing, northern boreal ecosystems may not compensate for the added greenhouse gas warming potential of methane in at least the short-term time frame (~100 years) given the relatively short lifespan of CH_4. In northwestern Canadian boreal peatlands, Helbig, Chasmer, Kljun, et al. (2017) estimated that

TABLE 3 Regression analysis of annual flux of net ecosystem exchange (NEE), gross primary productivity (GPP) and ecosystem respiration (total annual ER and winter ER) and best fit environmental variables for the years 2011–2022.

Flux ($g\,C\,m^{-2}\,year^{-1}$)	Site	Model	R^2	*p*-value	*N*
NEE	Black spruce	$16.70 - 0.868 \times (\text{total rain and SWE})_{\text{month prev}}$	0.50	<.0001	89
		$1315.705 - 4.459 \times \text{day of snow return}$	0.32	.08	10
		$1469.01 + 0.5982 \times \text{Total rain and SWE} - 5.7326 \times \text{day of snow return}$	0.49	.09	10
	Bog	$-28.0217 \times e^{x}$, where $x = 0.1981 \times T_{s_{\text{month prev}}}$	0.41	<.0001	60
		$-152.6805 + 0.4706 \times \text{total rain and SWE}$	0.45	.02	12
	Fen	$32.105 - 5.8467 \times T_{s_{\text{month}}}$	0.49	<.0001	84
		$-174.078 + 0.8433 \times \text{total rain}$	0.46	.03	11
		$31.477 - 34.105x + 0.0092x^2$, where $x = \text{GDDs}$	0.40	.02	11
	Old Bog	$4.826 - 273.738 \times T_{s_{\text{month}}}$	0.45	<.0001	31
GPP	Black spruce	$15.562 + 2.352 \times (\text{total rain} + \text{SWE})_{\text{month prev}}$	0.52	<.0001	89
		$-314.4681 - 2.1129 \times \text{total rain}$	0.67	.003	10
		$-47.2012 - 2.0017 \times \text{total rain and SWE}$	0.72	.001	10
		$-6.91263 - 0.10395 \times \text{winter } T_s$	0.60	.008	10
	Bog	$67.1358 \times e^{x}$, where $x = 0.0500 \times T_{s_{\text{month}}} + 0.00157 \times (\text{total rain and SWE})_{\text{month}}$	0.49	<.0001	60
		$-448.2220 - 0.5603 \times \text{total rain}$	0.74	.0004	12
	Fen	$25.411 + 12.433 \times T_{s_{\text{month}}} - 0.778 \times (\text{total rain and SWE})_{\text{month}} - 0.004 \times \{(\text{total rain and SWE})_{\text{month}} \times (T_{s_{\text{month}}})\}$	0.72	<.0001	84
		$-2026.697 + 4.965 \times \text{day of snow return}$	0.57	.01	11
	Old Bog	$18.3179 \times e^{x}$, where $x = 0.1673 \times T_{s_{\text{month}}}$	0.80	<.0001	31
ER	Black spruce	$35.241 + 1.440 \times (\text{total rain and SWE})_{\text{month prev}}$	0.32	<.0001	89
		$234.9425 + 2.5323 \times \text{total rain}$	0.67	.004	10
	Bog	$53.0093 \times e^{x}$, where $x = 0.0462 \times T_{s_{\text{month}}} + 0.00256 \times \text{total rain and SWE}_{\text{month}}$	0.35	<.0001	60
		$245.4551 + 0.9411 \times \text{total rain and SWE}$	0.67	<.0001	12
	Fen	$44.390 + 5.068 \times T_{s_{\text{month}}} - 0.291 \times \text{total rain and SWE}_{\text{month}} - 0.003 \times \{(\text{total rain and SWE})_{\text{month}} \times (T_{s_{\text{month}}})\}$	0.46	<.0001	84
		$1894.0318 + 0.7474 \times \text{total rain and SWE} - 5.3214 \times \text{day of snow return}$	0.40	.08	11
	Old Bog	$11.4066 \times e^{x}$, where $x = 0.1679 \times T_{s_{\text{month}}}$	0.66	<.0001	31
Winter ER	Black spruce	$40.1116 \times e^{x}$, where $x = 0.1579 \times T_{s_{\text{month}}} - 0.00324 \times (\text{total rain and SWE})_{\text{month}}$	0.35	<.0001	70
		$181.7969 \times e^{x}$, where $x = 0.1981 \times T_s$	0.54	.01	10
		$-11.05803 + 0.39970 \times \text{total rain}$	0.81	<.0001	10
	Bog	$17.1354 \times e^{x}$, where $x = 0.2813 \times T_{s_{\text{month}}}$	0.45	<.0001	84
		$-67.82487 + 0.39508 \times (\text{total rain and SWE})$	0.83	<.0001	12
		$89.4875 \times e^{x}$, where $x = 0.7057 \times T_s$	0.41	.03	12
		$30.229 + 0.4912 \times \text{total rain}$	0.49	.01	12
	Fen	$31.4231 \times e^{x}$, where $x = 0.3349 \times T_{s_{\text{month}}}$	0.31	<.0001	70
		$550.0047 + 0.5301 \times (\text{total rain and SWE}) - 2.0453 \times \text{day of snow return}$	0.51	.04	11
		$5.2481 \times e^{x}$, where $x = 0.4494 \times T_s$	0.52	.01	11
	Old Bog	$26.7905 \times e^{x}$, where $x = 0.1289 \times T_{s_{\text{month}}}$	0.52	.01	32

Note: The number of years used to construct the models of cumulative annual flux is $N = 12$ at the bog, $N = 11$ at the fen since data collection began in May 2011, and $N = 10$ at the black spruce site due to loosing data in 2014 and 2022 because of instrument malfunction. The old bog site is only included in the monthly analysis since data collection began in 2018. The subscript 'month' refers to values for a given variable from that current month and 'month prev' are values from the previous month. *p*-values below .05 are considered significant.

Abbreviations: GDD, growing degree days; SWE, snow water equivalent.

TABLE 4 Fixed effects models of moisture/inundation status and soil temperature (Equation 2) for NEE, ER, GPP ($g C m^{-2} day^{-1}$) and CH_4 ($g CH_4 m^{-2} day^{-1}$) at the rich fen.

Modeled flux	Status	Equation
NEE	Inundated May–June*	$0.27 - 0.10 \times T_s$
	Inundated July–September*	$3.57 - 0.40 \times T_s$
	Dry May–June*	$0.52 - 0.20 \times T_s$
	Dry July–September*	$2.17 - 0.27 \times T_s$
GPP	Inundated May–June*	$-0.85 - 0.34 \times T_s$
	Inundated July–September*	$1.47 - 0.48 \times T_s$
	Dry May–June*	$-1.33 - 0.31 \times T_s$
	Dry July–September*	$0.81 - 0.47 \times T_s$
ER	Inundated May–June*	$0.91 + 0.24 \times T_s$
	Inundated July–September*	$1.98 - 0.07 \times T_s$
	Dry May–June*	$1.72 + 0.12 \times T_s$
	Dry July–September*	$1.45 - 0.16 \times T_s$
CH_4	Inundated May–June	$0.002 + 0.005 \times T_s$
	Inundated July–September*	$-0.07 + 0.02 \times T_s$
	Dry May–June*	$-0.01 + 0.007 \times T_s$
	Dry July–September*	$-0.006 + 0.007 \times T_s$

Note: T_s = soil temperature at 7.5 cm depth. A '*' indicates the *p*-value for a given intercept and slope are statistically significant at $p < .05$. The degrees of freedom for the models of NEE, ER and GPP is 1817 and for the CH_4 model is 1354. Updated from Euskirchen et al. (2020).

a long-term net CO_2 uptake of >200 $g CO_2 m^2 year^{-1}$ is required to offset the positive radiative forcing of increasing CH_4 emissions until the end of the 21st century. The eddy covariance measurements of annual net CO_2 uptake in this northwestern Canadian landscape are less than half of this value at ~−78 $g CO_2 m^2 year^{-1}$ (Helbig, Chasmer, Kljun, et al., 2017), indicating CO_2 uptake cannot compensate for all emissions. In Sweden, year-round chamber measurements across a permafrost palsa, a *Sphagnum* bog underlain by permafrost, and a fully thawed fen, indicated that the landscape became a stronger CO_2 sink between 2012–2018, but future increases in CH_4 emissions due to permafrost thaw, greater inundation, and vegetation response could offset this sink, exerting a warming influence on the climate (Holmes et al., 2022). In a boreal forest in northern Sweden, 17 years of eddy covariance measurements of CO_2 from 1997 to 2013 indicated that the forest switched from a net C sink to C source due to increases in ecosystem respiration during both the spring and fall shoulder seasons (Hadden & Grelle, 2016). Our data show that from 2011 to 2022 the boreal lowlands of Interior Alaska were already net CO_2 sources due to larger releases of CO_2 through ER compared to uptake from GPP. Adding emissions of CH_4 results in large emissions expressed as CO_2 e (Figure 8). Thus, a number of studies under various methodologies found, including this study, demonstrate that thaw-induced increased CH_4 emissions, combined with possible decreases in net CO_2 uptake, should exert a positive net radiative greenhouse gas forcing through the 21st century.

4.2 | Trends, interannual variability and drivers of CO_2 fluxes

Despite trends in driving environmental variables, including warming soil temperatures, increased precipitation as both rain and snow, greater soil moisture, and a shorter snow season at our study sites from 2011 to 2022 (Figures 2–5), we did not find any statistically significant temporal trends (e.g., changes in the C sink strength of a site) in seasonal or annual C fluxes. However, as described below, the interannual variability of the C fluxes at our sites is large (i.e., Figure 6; Figure S1). It stands to reason that any trends in the data may be masked by the responses of these sites to shorter-term variations in biophysical variables and extreme events. This complication elicits the question of how many years of data would be needed to discern long-term trends arising from changes in driving factors linked to increases in atmospheric [CO_2] and climate warming from natural variability. Baldocchi et al. (2018) determined that measurement uncertainty is also a key factor in interpreting trends, with the detectable trend threshold needing to exceed 8 $g C m^{-2} year^{-1}$ with a measurement error of 30 $g C m^{-2} year^{-1}$ for a five-year time series. Our study shows uncertainty at these sites of 11–34 $g C m^2 year^{-1}$ (Table S3), indicating that given the length (~10 years) of our time series at the bog, black spruce, and fen sites, we should have been able to discern any temporal trends in the C fluxes against background measurement error.

The interannual variability of ecosystem C fluxes (represented as the standard deviation of the mean annual NEE over the number of measurement years; Figure 6) can represent vulnerability to variations in shorter term daily to seasonal weather patterns and extreme events. Large fluctuations in the C sink strength of an ecosystem due to these dynamics may have long-lasting influence on net C uptake at the decadal time scale. Here, we find that the interannual variability of the fen (±113 $g C m^{-2} year^{-1}$) and black spruce (±102 $g C m^{-2} year^{-1}$) was twice that reported for other boreal ecosystems, while that of the thermokarst bog (±58 $g C m^{-2} year^{-1}$) was close to reported values (±~40–50 $g C m^{-2} year^{-1}$; Alekseychik et al., 2021; Baldocchi et al., 2018; Launiainen et al., 2022; Strachan et al., 2016; Ueyama et al., 2014). This result indicates fluxes at the bog may be more resilient to shorter-term environmental changes such as flooding or snow. As previously reported in Euskirchen et al. (2020), interannual variability in the fen was primarily due to the record rainfall in 2014 when CO_2 release was 267 $g C m^{-2} year^{-1}$. The most recent measurements in 2022 also showed similar release of CO_2 at 251 $g C m^{-2} year^{-1}$, which was seemingly related to low GPP under early season inundated conditions at the site (354 $g C m^{-2} year^{-1}$; Table S3; Figure S4c). Unfortunately, data were lost in the black spruce in 2014 due to instrument malfunction, but the bog did show greater losses with the record rainfall (a more positive NEE) in 2014 compared to other years (124 $g C m^{-2}$; Figure S1).

Our year-round measurements of NEE provide an opportunity to better understand the importance and drivers of ecosystem respiration during the winter in this boreal landscape. Winter ER was between ~16%–24% of total annual ER (Figure 6), with variation in mean winter soil temperature exponentially related to total winter ER (Table 3).

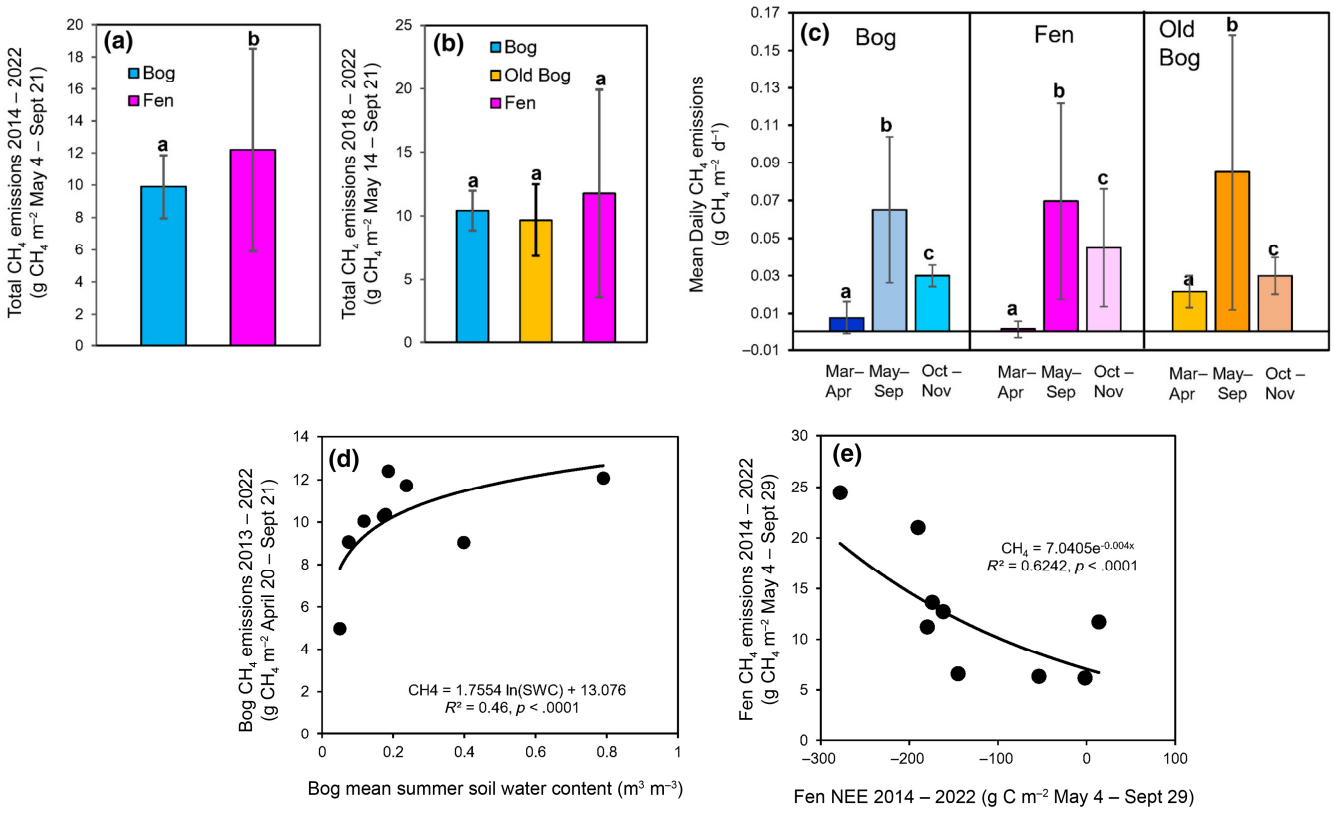

FIGURE 7 Total mean (standard deviation) daily emissions of CH_4 across periods of common data collection in the bog and fen (a) and the bog, old bog, and fen (b). In (c), mean (standard deviation) daily CH_4 emissions by seasons at the bog, fen, and old bog. In (d), relation between bog CH_4 emissions and water table depth, and in (e), the relation between CH_4 emissions and NEE. Different letters indicate significant differences between sites for a given flux based on a Games-Howell test.

We also found greater winter ER occurred following wetter summers (Table 3) demonstrating how summer conditions can influence winter processes. This relationship is particularly notable given that each year from 2014 was marked by total rainfall that was greater than the mean (Figure 2a) and that increases in precipitation, as both rain and snow, are generally expected under a warming climate (Bintanja & Andry, 2017). Increases in precipitation as snow may result in a deeper snowpack with warmer temperatures and a deepening active layer depth which can support increasing rates of microbial activity over winter (Natali et al., 2019). Soil temperature was a significant predictor of winter ER at all sites and SWE was a significant predictor at the bog and fen (Table 3). In the future, it will be valuable to explore the relationship between year-round NEE and active layer depth, but at present, the ALD data and C fluxes for the individual sites do not align for a long enough period of time to perform this analysis. It is therefore critical to continue to explore winter dynamics and the processes that may enhance or impede winter respiration in boreal landscapes since this may have a significant impact on boreal carbon budgets.

4.3 | Drivers of CH_4

The significant differences in mean total CH_4 emissions from 2014 to 2022 between the bog and fen (Figure 6a) resulted in cumulative CH_4 + NEE emissions (Figure 8) at the fen (5263 g CO_2 e m^{-2}) that were larger than those at the bog (4210 g CO_2 e m^{-2}), with likely an even larger estimate at the fen because CH_4 measurements at the fen began a year later (2014 vs. 2013). However, we also found that winter emissions of CH_4 (based on measurements in late March and early April when soils were frozen; Figure 7c) are likely less than those of the bog (2% of May–September emissions at the fen versus 10% at the bog). Future work at these sites would benefit from mechanistic biogeochemical and microbial studies in addition to year-round CH_4 measurements, similar to the investigations of Rinne et al. (2018) in boreal Finland, but would necessitate an augmentation of the power supply or more frequent generator use in the winter. It would also be helpful to compare long-term measurements between closed-path and open-path analyzers at these sites given longer path lengths and necessary air density corrections associated with open-path analyzers. However, recent work finds good agreement between the two sensor types over the long-term, with more error due to the stochasticity of turbulent transport and flux footprint heterogeneity than due to the different types of analyzers (Deventer et al., 2019).

While water table depth strongly affects CH_4 release in peatlands (Huang et al., 2021; Knox et al., 2021; Moore & Roulet, 1993), we did not observe this relation at either of our sites because (1) the fen was often flooded (Figure 3b) and (2) the bog contains a

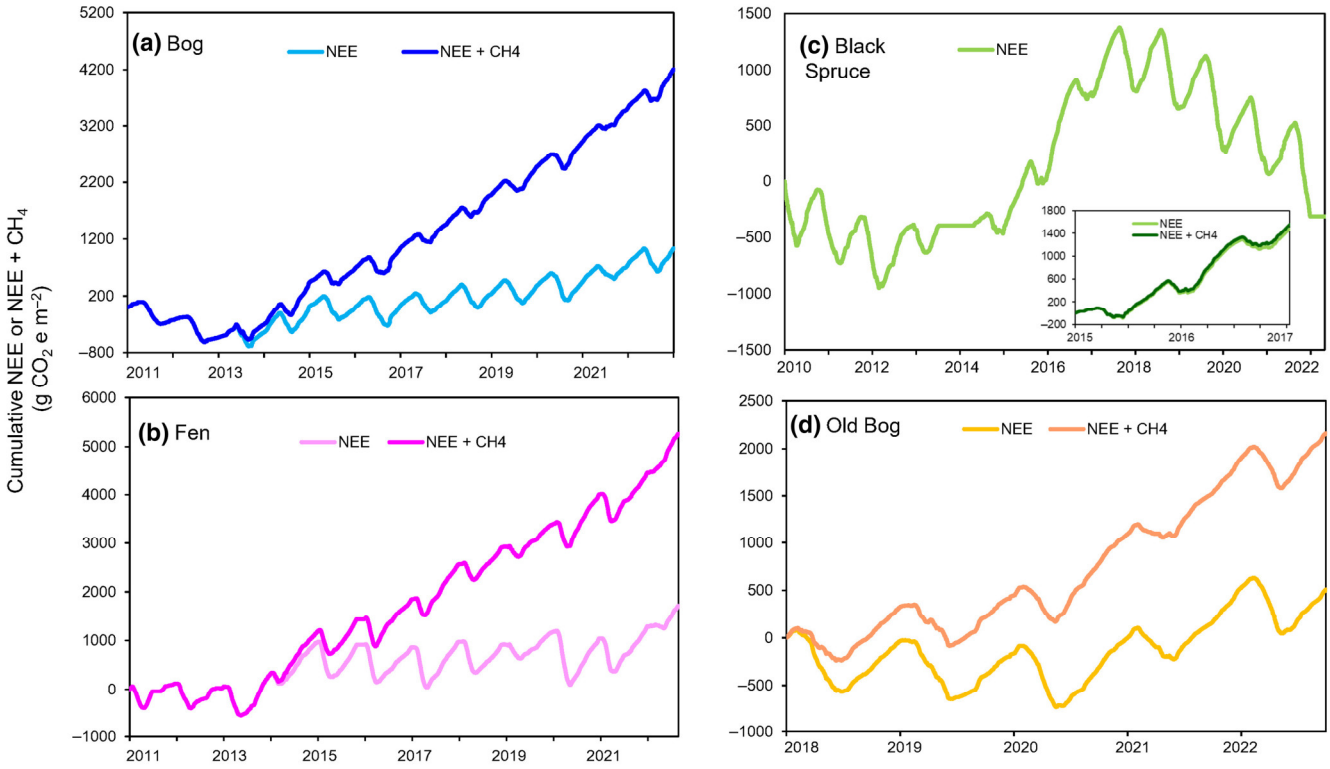

FIGURE 8 Cumulative net ecosystem exchange (NEE) and NEE + CH_4 expressed as CO_2 equivalents (CO_2 e) for the bog (a), rich fen (b), black spruce (c), and old bog (d). These graphs include all time periods when both NEE and CH_4 data were collected at the sites.

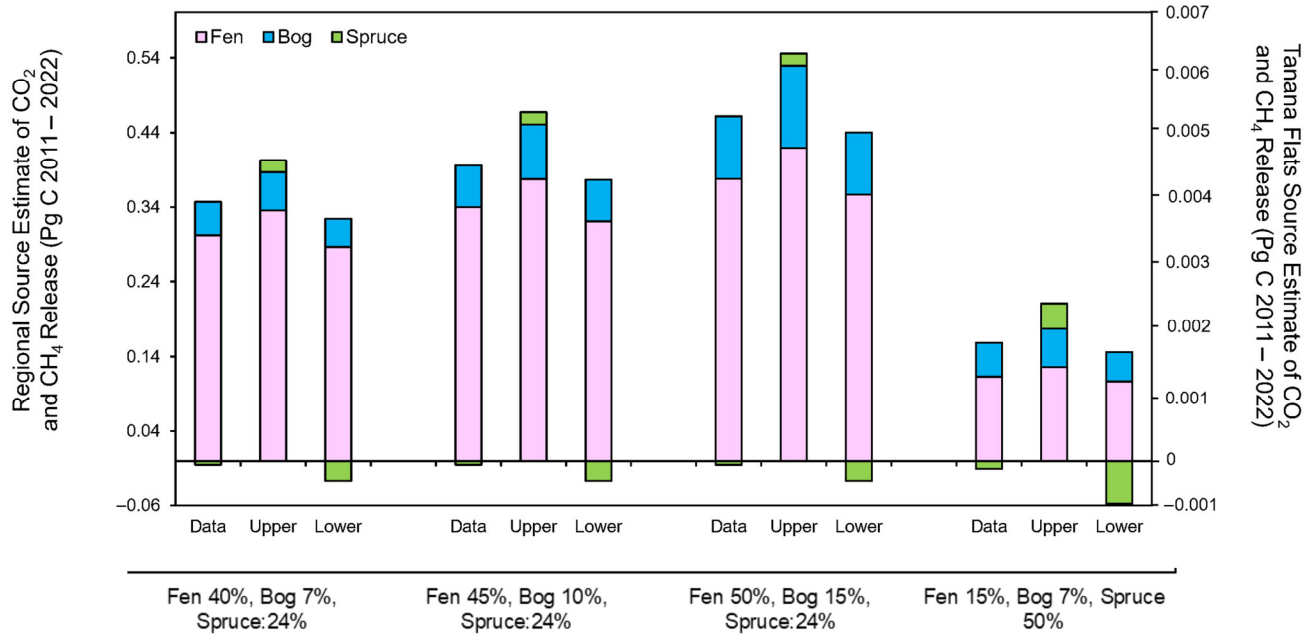

FIGURE 9 Estimate of CO_2 and CH_4 release across the boreal lowland region in Interior, AK and for the Tanana Flats for the years of our measurements from 2011 to 2022 as shown in Figure 7. Estimates are based on the data provided in Figure 7, indicated by 'Data' and also on the 'Upper' and 'Lower' end of the errors provided in Table S3.

floating peat mat, such that measured water table depth can seem quite stable despite variation in site hydrology (Figure 3a). However, at the bog we did find a relationship between soil water content in shallow soil (5 cm) and total CH_4 emissions from May to September (Figure 7d). In agreement with Euskirchen et al. (2020), we found that flooding in the fen during the early season was related to smaller CH_4 emissions, while flooding later in the season was related to larger CH_4 emissions. This trend could be due to at least three

possible explanations (see also Euskirchen et al., 2020). First, a high water table can reduce CH_4 emissions because the aerenchymatous plants (sedges, horsetail, grasses) that dominate this ecosystem are submerged—thereby negating their ability to "pipe" CH_4 to the atmosphere. Second, an increase in the activity of aerenchymatous plants during flooding can have an oxidizing effect on rhizosphere pore water chemistry, producing an environment more favorable for methanotrophy during the growing season, (McPartland et al., 2019; Rupp et al., 2019; Strack et al., 2017). Third, flooding may affect redox chemistry, increasing soil ferric iron and nitrate for example, thereby suppressing methanogenesis (Mitchell & Branfireun, 2005). The relation between NEE and CH_4 emissions at the fen also suggests a rhizodeposition effect, where greater net CO_2 uptake corresponds to greater release of CH_4, which could be caused by feeding of methanogens in the rhizosphere of growing plants, and the seasonal dynamics of facultative methane oxidizers (Rupp et al., 2021; Turner et al., 2020; Figure 7e).

4.4 | Wetland type and landscape mapping: Implications for C cycling in landscapes undergoing permafrost thaw

As widespread permafrost thaw continues over this century (Douglas et al., 2021), the areal coverage of different ecosystems will change, sometimes in unpredictable ways, altering regional C budgets. For example, recent work suggests that talik formation (unfrozen zones either above or within the permafrost soil layers) and talik thickness in black spruce lowland areas will increase substantially and could impact up to 70% of the Interior Alaska landscape (Farquharson et al., 2022), thereby influencing thermokarst development, hydrological connectivity, and carbon cycling. The significance of accurate landscape mapping of poorly drained, lowland peatlands undergoing permafrost thaw is highlighted by large differences in estimates of C losses from boreal lowlands in Interior Alaska due to differences in ecosystem type (Figure 9). Other work has also emphasized the importance of maps that delineate bogs and fens (Jorgenson et al., 2001), with significantly greater CH_4 emissions found in fens compared to bogs in the boreal region (Turetsky et al., 2014) and a greater sensitivity of fens compared to bogs to climate change (Wu & Roulet, 2014), as also found in this study. While we did not find significant differences in C fluxes between the bog and old bog based on our 3 years of data (Figures 6 and 7), other work has highlighted the ecological diversity of bogs across the boreal region and suggests that different types of bogs should be delineated, including pine bogs compared to bogs with dwarf shrubs and sphagnum (Alekseychik et al., 2021) or bogs that have rapidly expanded following fire (Gibson et al., 2018).

It is important to accurately delineate the proportion of the landscape covered by ecosystems with low CH_4 emissions, such as our black spruce site (Figure 8c), and high CO_2 uptake, such as some mature boreal forests (Peichl et al., 2023), including the upland white spruce and birch/aspen forests that we do not measure. It should also be noted that our flux towers lie with a ~1 km^2 section of the landscape, and as such, landscape heterogeneity at this scale should be considered in both mapping and modeling efforts. In addition, while the fen, bog, and black spruce ecosystems studied here are considered representative of those across the lowlands in boreal Alaska, additional long-term eddy covariance measurements in other lowland wetland complexes in boreal Alaska would help to elucidate how well they do indeed represent the landscape. Modeling studies of lowland boreal wetland biogeochemistry in Alaska are relatively rare, but they find, similar to this study, that this landscape is a net source of C (Lyu et al., 2018; Ma et al., 2023). However, these modeling studies include shortcomings, including the inability to delineate and model fens versus bogs, parameterizations based on historical data from Canadian wetlands without considering the most recent data from boreal Alaska or only a simple representation of permafrost. Our upscaling analysis presented here, combined with the shortcomings of published modeling studies in this landscape, point to the importance and need for a more detailed modeling approach in these boreal lowlands.

While this study considers the contribution of net CO_2 and CH_4 emissions to climate warming from lowland boreal ecosystems, a fully upscaled C balance of this landscape would need to consider other factors. For example, dissolved organic carbon from the fen could increase lateral C losses (Kane et al., 2010; Roulet et al., 2007). Some losses may, in part, be counterbalanced by increases in nitrogen availability as permafrost thaws, thereby promoting greater plant productivity (Finger et al., 2016). Furthermore, it is important to consider the plant component of ecosystem respiration since increasing CO_2 emissions could also be related to increasing aboveground plant respiration (King et al., 2006). Other climate feedbacks, such as increases in evapotranspiration (Helbig et al., 2020) and decreases in snow cover (Euskirchen et al., 2016), would provide an even more inclusive picture of the atmospheric warming potential of boreal lowlands.

Finally, the fate of permafrost C post thaw depends on the history of permafrost formation. Sites with older syngenetic permafrost, or permafrost that aggraded at the same time as the peat formed, typically have carbon rich soils with well-preserved organic matter and can correspond to post-thaw carbon losses of 45 kg C m^{-2} in the century following thaw (Jones et al., 2017). Alternatively, epigenetic permafrost, or permafrost that aggraded after the peat formed, at our site and in many boreal peatlands is younger and formed after peat accumulation, meaning permafrost organic matter is more processed. At these sites, post-thaw carbon losses tend to be smaller, ranging from 20 kg C m^{-2} to 27 kg C m^{-2} in the century following thaw (Manies et al., 2021). These losses can be partially or fully offset from the higher rates of C accumulation in the post-thaw bogs compared to the permafrost forests (Estop-Aragonés et al., 2018). Therefore, when extrapolating estimates of C release across boreal lowlands, consideration should be given to how and when the permafrost aggraded as it may influence present-day estimates of C release and uptake.

5 | CONCLUSION

Our work illustrates the importance of long-term measurements of carbon fluxes over the full annual cycle in heterogeneous boreal lowlands undergoing unprecedented shifts in climate, permafrost thaw, and changing hydrology. Based on these measurements, it would be valuable to reconsider our paradigm of boreal landscapes as net carbon sinks, particularly as the landscape shifts to a greater coverage of area occupied by wetlands, and fens in particular, as permafrost continues to thaw. This work also has implications for ecosystem modeling in this region, with larger interannual variability than found in other boreal ecosystems, coupled with the prevalence of extreme events, ongoing warming, and increases in both rain in snow. These factors contribute to larger uncertainty bounds for model benchmarks and illustrate the importance of assimilating the most recent carbon flux measurements for quantifying boreal carbon balance under a rapidly changing climate.

AUTHOR CONTRIBUTIONS

Eugénie S. Euskirchen: Conceptualization; data curation; formal analysis; funding acquisition; investigation; methodology; writing – original draft; writing – review and editing. **Colin Edgar:** Data curation; formal analysis; investigation; methodology; writing – original draft; writing – review and editing. **Evan S. Kane:** Conceptualization; funding acquisition; writing – original draft; writing – review and editing. **Mark P. Waldrop:** Conceptualization; funding acquisition; writing – original draft; writing – review and editing. **Rebecca B. Neumann:** Investigation; writing – original draft; writing – review and editing. **Kristen Manies:** Data curation; formal analysis; methodology; writing – original draft; writing – review and editing. **Thomas Douglas:** Data curation; methodology; writing – original draft; writing – review and editing. **Catherine Dieleman:** Data curation; investigation; writing – original draft; writing – review and editing. **Miriam Jones:** Data curation; formal analysis; investigation; methodology; writing – original draft; writing – review and editing. **merritt turetsky:** Conceptualization; funding acquisition; methodology; writing – original draft; writing – review and editing.

ACKNOWLEDGEMENTS

This project was funded by the National Science Foundation Grants DEB LTREB 1354370 and 2011257, DEB-0425328, DEB-0724514, and DEB-0830997. The Bonanza Creek Long Term Experimental Research station provided lab space, equipment, and time to this project. T. Douglas was funded by the Department of Defense's Strategic Environmental Research and Development Program (Project RC-2110) and the U.S. Army Corps of Engineers Engineer Research and Development Center's Basic Research (6.2) Program under 0602182 A/Network C3I Enabling Technologies. This research was also funded by the US Geological Survey Climate R&D program and received in-kind support from the USDA Forest Service Northern Research Station. Any use of trade, firm, or product names is for descriptive purposes only and does not imply endorsement by the U.S. Government.

CONFLICT OF INTEREST STATEMENT

The authors declare no competing financial interest.

DATA AVAILABILITY STATEMENT

The data that support the findings of this study are openly available through Ameriflux: https://ameriflux.lbl.gov/ at: https://doi.org/10.17190/AMF/1756433; https://doi.org/10.17190/AMF/1756434; https://doi.org/10.17190/AMF/1773401; https://doi.org/10.17190/AMF/1846662.

ORCID

Eugénie S. Euskirchen https://orcid.org/0000-0002-0848-4295
Catherine Dieleman https://orcid.org/0000-0002-4280-5849

REFERENCES

Alekseychik, P., Korrensalo, A., Mammarella, I., Launiainen, S., Tuittila, E.-S., Korpela, I., & Vesala, T. (2021). Carbon balance of a Finnish bog: Temporal variability and limiting factors based on 6 years of eddy-covariance data. *Biogeosciences*, *18*, 4681–4704. https://doi.org/10.5194/bg-18-4681-2021

Baldocchi, D. D., Chua, H., & Reichsteinb, M. (2018). Inter-annual variability of net and gross ecosystem carbon fluxes: A review. *Agricultural and Forest Meteorology*, *249*, 520–533. https://doi.org/10.1016/j.agrformet.2017.05.015

Bintanja, R., & Andry, O. (2017). Towards a rain-dominated Arctic. *Nature Climate Change*, *7*, 263–267. https://doi.org/10.1038/nclimate3240

Bradshaw, C., & Warkentin, I. (2015). Global estimates of boreal forest carbon stocks and flux. *Global and Planetary Change*, *128*, 24–30. https://doi.org/10.1016/j.gloplacha.2015.02.004

Camill, P., Lynch, J. A., Clark, J. S., Adams, J. B., & Jordan, B. (2001). Changes in biomass, aboveground net primary production, and peat accumulation following permafrost thaw in the boreal peatlands of Manitoba, Canada. *Ecosystems*, *4*, 461–478. https://doi.org/10.1007/s10021-001-0022-3

Charman, D. J., Beilman, D. W., Blaauw, M., Booth, R. K., Brewer, S., Chambers, F. M., Christen, J. A., Gallego-Sala, A., Harrison, S. P., Hughes, P. D. M., Jackson, S. T., Korhola, A., Mauquoy, D., Mitchell, F. J. G., Prentice, I. C., van der Linden, M., de Vleeschouwer, F., Yu, Z. C., Alm, J., … Zhao, Y. (2013). Climate-related changes in peatland carbon accumulation during the last millennium. *Biogeosciences*, *10*, 929–944. https://doi.org/10.5194/bg-10-929-2013

Chivers, M. R., Turetsky, M. R., Waddington, J. M., Harden, J. W., & McGuire, A. D. (2009). Effects of experimental water table and temperature manipulations on ecosystem CO_2 fluxes in an Alaskan rich fen. *Ecosystems*, *12*, 1329–1342. https://doi.org/10.1007/s10021-009-9292-y

Christensen, T. R., Johansson, T., Akerman, H. J., & Mastepanov, M. (2004). Thawing sub-arctic permafrost: Effects on vegetation and methane emissions. *Geophysical Research Letters*, *31*, 1–4. https://doi.org/10.1029/2003GL018680

Christensen, T. R., Johansson, T., Olsrud, M., Ström, L., Lindroth, A., Mastepanov, M., Malmer, N., Friborg, T., Crill, P., & Callaghan, T. V. (2007). A catchment-scale carbon and greenhouse gas budget of a subarctic landscape. *Philosophical Transactions. Series A: Mathematical, Physical, and Engineering Science*, *365*, 1643–1656. https://doi.org/10.1098/rsta.2007.2035

Davidson, E. A., & Janssens, I. A. (2006). Temperature sensitivity of soil carbon decomposition and feedbacks to climate change. *Nature*, *440*, 165–173. https://doi.org/10.1038/nature04514

Delwiche, K. B., Knox, S. H., Malhotra, A., Fluet-Chouinard, E., McNicol, G., Feron, S., Ouyang, Z., Papale, D., Trotta, C., Canfora, E., Cheah,

Y. W., Christianson, D., Alberto, M. C. R., Alekseychik, P., Aurela, M., Baldocchi, D., Bansal, S., Billesbach, D. P., Bohrer, G., … Jackson, R. B. (2021). FLUXNET-CH4: A global, multi-ecosystem dataset and analysis of methane seasonality from freshwater wetlands. *Earth System Science Data*, *13*, 3607–3689. https://doi.org/10.5194/essd-13-3607-2021

Deventer, M. J., Griffis, T. J., Roman, D. T., Kolka, R. K., Wood, J. D., Erickson, M., Baker, J. M., & Millet, D. B. (2019). Error characterization of methane fluxes and budgets derived from a long-term comparison of open- and closed-path eddy covariance systems. *Agricultural and Forest Meteorology*, *279*, 1–15. https://doi.org/10.1016/j.agrformet.2019.107638

Douglas, T. A., Hiemstra, C. A., Anderson, J. E., Barbato, R. A., Bjella, K. L., Deeb, E. J., Gelvin, A. B., Nelsen, P. E., Newman, S. D., Saari, S. P., & Wagner, A. M. (2021). Recent degradation of Interior Alaska permafrost mapped with ground surveys, geophysics, deep drilling, and repeat airborne lidar. *The Cryosphere*, *15*, 3555–3575. https://doi.org/10.5194/tc-15-3555-2021

Douglas, T. A., Jones, M. C., Hiemstra, C. A., & Arnold, J. R. (2014). Sources and sinks of carbon in boreal ecosystems of Interior Alaska: A review. *Elementa: Science of the Anthropocene*, *2*, 000032. https://doi.org/10.12952/journal.elementa.000032

Douglas, T. A., Turetsky, M. R., & Koven, C. D. (2020). Increased rainfall stimulates permafrost thaw across a variety of Interior Alaskan boreal ecosystems. *npj Climate and Atmospheric Science*, *3*, 28. https://doi.org/10.1038/s41612-020-00155-6

Estop-Aragonés, C., Cooper, M. D. A., Fisher, J. P., Thierry, A., Garnett, M. H., Charman, D. J., Murton, J. B., Phoenix, G. K., Treharne, R., Sanderson, N. K., Burn, C. R., Kokelj, S. V., Wolfe, S. A., Lewkowicz, A. G., Williams, M., & Hartley, I. P. (2018). Limited release of previously-frozen C and increased new peat formation after thaw in permafrost peatlands. *Soil Biology and Biochemistry*, *118*, 115–129. https://doi.org/10.1016/j.soilbio.2017.12.010

Euskirchen, E. (2022a). AmeriFlux BASE US-BZB Bonanza Creek Thermokarst Bog, Ver. 4-5, AmeriFlux AMP [Data set]. https://doi.org/10.17190/AMF/1773401

Euskirchen, E. (2022b). AmeriFlux BASE US-BZS Bonanza Creek Black Spruce, Ver. 3-5, AmeriFlux AMP [Data set]. https://doi.org/10.17190/AMF/1756434

Euskirchen, E. (2022c). AmeriFlux BASE US-BZF Bonanza Creek Rich Fen, Ver. 4-5, AmeriFlux AMP [Data set]. https://doi.org/10.17190/AMF/1756433

Euskirchen, E. (2022d). AmeriFlux BASE US-BZo Bonanza Creek Old Thermokarst Bog, Ver. 3-5, AmeriFlux AMP [Data set]. https://doi.org/10.17190/AMF/1846662

Euskirchen, E. S., Bennett, A., Breen, A. L., Genet, H., Lindgren, M., Kurkowski, T., McGuire, A. D., & Rupp, T. S. (2016). Consequences of changes in vegetation and snow cover for climate feedbacks in Alaska and northwest Canada. *Environmental Research Letters*, *11*, 105003. https://doi.org/10.1088/1748-9326/11/10/105003

Euskirchen, E. S., Bret-Harte, M. S., Shaver, G. R., Edgar, C. W., & Romanovsky, V. E. (2017). Long-term release of carbon dioxide from arctic tundra ecosystems in northern Alaska. *Ecosystems*, *20*, 960–974. https://doi.org/10.1007/s10021-016-0085-9

Euskirchen, E. S., Edgar, C., Turetsky, M. R., Waldrop, M. P., & Harden, J. W. (2014). Differential response of carbon fluxes to climate in three peatland ecosystems that vary in the presence and stability of permafrost. *Journal of Geophysical Research: Biogeosciences*, *119*, 1576–1595. https://doi.org/10.1002/2014JG002683

Euskirchen, E. S., Kane, E. S., Edgar, C. W., & Turetsky, M. R. (2020). When the source of flooding matters: Divergent responses in carbon fluxes in an Alaskan rich fen to two types of inundation. *Ecosystems*, *23*, 1138–1153. https://doi.org/10.1007/s10021-019-00460-z

Falge, E., Baldocchi, D., Olson, R., Anthoni, P., Aubinet, M., Bernhofer, C., Burba, G., Ceulemans, R., Clement, R., Dolman, H., Granier, A., Gross, P., Grünwald, T., Hollinger, D., Jensen, N. O., Katul, G., Keronen, P., Kowalski, A., Lai, C. T., … Wofsy, S. (2001). Gap filling strategies for defensible annual sums of net ecosystem exchange. *Agricultural and Forest Meteorology*, *107*, 43–69. https://doi.org/10.1016/S0168-1923(00)00225-2

Farquharson, L. M., Romanovsky, V. E., Kholodov, A., & Nicolsky, D. (2022). Sub-aerial talik formation observed across the discontinuous permafrost zone of Alaska. *Nature Geoscience*, *15*, 475–481. https://doi.org/10.1038/s41561-022-00952-z

Finger, R. A., Turetsky, M. R., Kielland, K., Ruess, R. W., Mack, M. C., & Euskirchen, E. S. (2016). Effects of permafrost thaw on nitrogen availability and plant-soil interactions in a boreal Alaskan lowland. *Journal of Ecology*, *104*, 1542–1554. https://doi.org/10.1111/1365-2745.12639

Frolking, S., Talbot, J., Jones, M. C., Treat, C. C., Kauffman, J. B., Tuittila, E.-S., & Roulet, N. T. (2011). Peatlands in the Earth's 21st century climate system. *Environmental Reviews*, *19*, 371–396. https://doi.org/10.1139/a11-014

Gibson, C. M., Chasmer, L. E., Thompson, D. K., Quinton, W. L., Flannigan, M. D., & Olefeldt, D. (2018). Wildfire as a major driver of recent permafrost thaw in boreal peatlands. *Nature Communications*, *9*, 3041. https://doi.org/10.1038/s41467-018-05457-1

Gorham, E. (1991). Northern peatlands: Role in the carbon cycle and probable responses to climatic warming. *Ecological Applications*, *1*, 182–195. https://doi.org/10.2307/1941811

Hadden, D., & Grelle, A. (2016). Changing temperature response of respiration turns boreal forest from carbon sink into carbon source. *Agricultural and Forest Meteorology*, *223*, 30–38. https://doi.org/10.1016/j.agrformet.2016.03.020

Heffernan, L., Cavaco, M. A., Bhatia, M. P., Estop-Aragones, C., Knor, K.-H., & Olefeldt, D. (2022). High peatland methane emissions following permafrost thaw: Enhanced acetoclastic methanogenesis during early successional stages. *Biogeosciences*, *19*, 3051–3071. https://doi.org/10.5194/bg-19-3051-2022

Heiskanen, L., Tuovinen, J. P., Räsänen, A., Virtanen, T., Juutinen, S., Lohila, A., Penttilä, T., Linkosalmi, M., Mikola, J., Laurila, T., & Aurela, M. (2021). Carbon dioxide and methane exchange of a patterned subarctic fen during two contrasting growing seasons. *Biogeosciences*, *18*, 873–896. https://doi.org/10.5194/bg-18-873-2021

Helbig, M., Chasmer, L. E., Desai, A. R., Kljun, N., Quinton, W. L., & Sonnentag, O. (2017). Direct and indirect climate change effects on carbon dioxide fluxes in a thawing boreal forest-wetland landscape. *Global Change Biology*, *23*, 3231–3248. https://doi.org/10.1111/gcb.13638

Helbig, M., Chasmer, L. E., Kljun, N., Quinton, W. L., Treat, C. C., & Sonnentag, O. (2017). The positive net radiative greenhouse gas forcing of increasing methane emissions from a thawing boreal forest-wetland landscape. *Global Change Biology*, *23*, 2413–2427. https://doi.org/10.1111/gcb.13520

Helbig, M., Waddington, J. M., Alekseychik, P., Amiro, B. D., Aurela, M., Barr, A. G., Black, T. A., Blanken, P. D., Carey, S. K., Chen, J., Chi, J., Desai, A. R., Dunn, A., Euskirchen, E. S., Flanagan, L. B., Forbrich, I., Friborg, T., Grelle, A., Harder, S., … Zyrianov, V. (2020). Increasing contribution of peatlands to boreal evapotranspiration in a warming climate. *Nature Climate Change*, *10*, 555–560. https://doi.org/10.1038/s41558-020-0763-7

Heskel, M. A., O'Sullivan, O. S., Reich, P. B., Tjoelker, M. G., Weerasinghe, L. K., Penillard, A., Egerton, J. J. G., Creek, D., Bloomfield, K. J., Xiang, J., Sinca, F., Stangl, Z. R., Martinez-de la Torre, A., Griffin, K. L., Huntingford, C., Hurry, V., Meir, P., Turnbull, M. H., & Atkin, O. K. (2016). Convergence in the temperature response of leaf respiration across biomes and plant functional types. *Proceedings of the National Academy of Sciences of the United States of America*, *113*, 3832–3837. https://doi.org/10.1073/pnas.1520282113

Holmes, M. E., Crill, P. M., Burnett, W. C., McCalley, C. K., Wilson, R. M., Frolking, S., Chang, K. Y., Riley, W. J., Varner, R. K., Hodgkins, S. B.,

IsoGenie Project Coordinators, IsoGenie Field Team, McNichol, A. P., Saleska, S. R., Rich, V. I., & Chanton, J. P. (2022). Carbon accumulation, flux, and fate in Stordalen Mire, a permafrost peatland in transition. *Global Biogeochemical Cycles*, *36*, e2021GB007113. https://doi.org/10.1029/2021GB007113

Huang, Y., Ciais, P., Luo, Y., Zhu, D., Wang, Y., Qiu, C., Goll, D. S., Guenet, B., Makowski, D., de Graaf, I., Leifeld, J., Kwon, M. J., Hu, J., & Qu, L. (2021). Tradeoff of CO_2 and CH_4 emissions from global peatlands under water-table drawdown. *Nature Climate Change*, *11*, 618–622. https://doi.org/10.1038/s41558-021-01059-w

Hugelius, G., Loisel, J., Chadburn, S., Jackson, R. B., Jones, M., MacDonald, G., Marushchak, M., Olefeldt, D., Packalen, M., Siewert, M. B., Treat, C., Turetsky, M., Voigt, C., & Yu, Z. (2020). Large stocks of peatland carbon and nitrogen are vulnerable to permafrost thaw. *Proceedings of the National Academy of Sciences of the United States of America*, *117*, 20438–20446. https://doi.org/10.1073/pnas.1916387117

Jones, M. C., Booth, R. K., Yu, Z., & Ferry, P. (2012). A 2200-year record of permafrost dynamics and carbon cycling in a collapse-scar bog, Interior Alaska. *Ecosystems*, *16*, 1–19. https://doi.org/10.1007/s10021-012-9592-5

Jones, M. C., Grosse, G., Treat, C., Turetsky, M., Walter Anthony, K., & Brosius, L. (2023). Past permafrost dynamics can inform future permafrost carbon-climate feedbacks. *Communications Earth and Environment*, *4*, 272. https://doi.org/10.1038/s43247-023-00886-3

Jones, M. C., Harden, J., O'Donnell, J., Manies, K., Jorgenson, T., Treat, C., & Ewing, S. (2017). Rapid carbon loss and slow recovery following permafrost thaw in boreal peatlands. *Global Change Biology*, *23*, 1109–1127. https://doi.org/10.1111/gcb.13403

Jorgenson, M. T., Brown, D. R., Hiemstra, C. A., Genet, H., Marcot, B. G., Murphy, R. J., & Douglas, T. A. (2022). Drivers of historical and projected changes in diverse boreal ecosystems: Fires, thermokarst, riverine dynamics, and humans. *Environmental Research Letters*, *17*, 045016. https://doi.org/10.1088/1748-9326/ac5c0d

Jorgenson, M. T., Douglas, T. A., Liljedahl, A. K., Roth, J. E., Cater, T. C., Davis, W. A., Frost, G. V., Miller, P. F., & Racine, C. H. (2020). The roles of climate extremes, ecological succession, and hydrology in repeated permafrost aggradation and degradation in fens on the Tanana Flats, Alaska. *Journal of Geophysical Research: Biogeosciences*, *125*, e2020JG005824. https://doi.org/10.1029/2020JG005824

Jorgenson, M. T., & Osterkamp, T. E. (2005). Response of boreal ecosystems to varying modes of permafrost degradation. *Canadian Journal of Forest Research*, *35*, 2100–2111. https://doi.org/10.1139/x05-153

Jorgenson, M. T., Racine, C. H., Walters, J. C., & Osterkamp, T. E. (2001). Permafrost degradation and ecological changes associated with a warming climate in central Alaska. *Climatic Change*, *48*, 551–579. https://doi.org/10.1023/A:1005667424292

Jorgenson, M. T., Romanovsky, V. R., Harden, J., Shur, Y., O'Donnell, J. O., Schuur, E. A., Kanevskiy, M. Z., & Marchenko, S. S. (2010). Resilience and vulnerability of permafrost to climate change. *Canadian Journal of Forest Research*, *40*, 1219–1236. https://doi.org/10.1139/X10-060

Kane, E. S., Turetsky, M. R., Harden, J. W., McGuire, A. D., & Waddington, J. M. (2010). Seasonal ice and hydrological controls on dissolved organic carbon and nitrogen concentrations in a boreal-rich fen. *Journal of Geophysical Research*, *115*, 1–15. https://doi.org/10.1029/2010JG001366

King, A. W., Gunderson, C. A., Post, W. M., Weston, D. J., & Wullschleger, S. D. (2006). Plant respiration in a warmer world. *Science*, *312*, 536–537. https://doi.org/10.1126/science.111416

Knox, S. H., Bansal, S., McNicol, G., Schafer, K., Sturtevant, C., Ueyama, M., Valach, A. C., Baldocchi, D., Delwiche, K., Desai, A. R., Euskirchen, E., Liu, J., Lohila, A., Malhotra, A., Melling, L., Riley, W., Runkle, B. R. K., Turner, J., Vargas, R., … Jackson, R. B. (2021). Identifying dominant environmental predictors of freshwater wetland methane fluxes across diurnal to seasonal time scales. *Global Change Biology*, *27*, 3582–3604. https://doi.org/10.1111/gcb.15661

Laine, A. M., Mäkiranta, P., Laiho, R., Mehtätalo, L., Penttilä, T., Korrensalo, A., Minkkinen, K., Fritze, H., & Tuittila, E.-S. (2019). Warming impacts on boreal fen CO_2 exchange under wet and dry conditions. *Global Change Biology*, *2019*, 1995–2008. https://doi.org/10.1111/gcb.14617

Lara, M. J., Genet, H., McGuire, A. D., Euskirchen, E. S., Zhang, Y., Brown, D. R., Jorgenson, M. T., Romanovsky, V. E., Breen, A. L., & Bolton, W. R. (2016). Thermokarst rates intensify due to climate change and forest fragmentation in an Alaskan boreal forest lowland. *Global Change Biology*, *22*, 816–829. https://doi.org/10.1111/gcb.13124

Launiainen, S., Katul, G. G., Leppä, K., Kolari, P., Aslan, T., Grönholm, T., Korhonen, L., Mammarella, I., & Vesala, T. (2022). Does growing atmospheric CO_2 explain increasing carbon sink in a boreal coniferous forest? *Global Change Biology*, *28*, 2910–2929. https://doi.org/10.1111/gcb.16117

Lehmann, J., & Coumou, D. (2015). The influence of mid-latitude storm tracks on hot, cold, dry and wet extremes. *Scientific Reports*, *5*, 17491. https://doi.org/10.1038/srep17491

Liu, P., Black, T. A., Jassal, R. S., Zha, T., Nesic, Z., Barr, A. G., Helgason, W. D., Jia, X., Tian, Y., Stephens, J. J., & Ma, J. (2019). Divergent long-term trends and interannual variation in ecosystem resource use efficiencies of a southern boreal old black spruce forest 1999–2017. *Global Change Biology*, *25*, 3056–3069. https://doi.org/10.1111/gcb.14674

Liu, Z., Kimball, J. S., Ballantyne, A. P., Parazoo, N. C., Wang, W. J., Bastos, A., Madani, N., Natali, S. M., Watts, J. D., Rogers, B. M., Ciais, P., Yu, K., Virkkala, A. M., Chevallier, F., Peters, W., Patra, P. K., & Chandra, N. (2022). Respiratory loss during late-growing season determines the net carbon dioxide sink in northern permafrost regions. *Nature Communications*, *13*, 5626. https://doi.org/10.1038/s41467-022-33293-x

Lloyd, J., & Taylor, J. A. (1994). On the temperature dependence of soil respiration. *Functional Ecology*, *8*, 315. https://doi.org/10.2307/2389824

Loisel, J., Gallego-Sala, A. V., Amesbury, M. J., Magnan, G., Anshari, G., Beilman, D. W., Benavides, J. C., Blewett, J., Camill, P., Charman, D. J., Chawchai, S., Hedgpeth, A., Kleinen, T., Korhola, A., Large, D., Mansilla, C. A., Müller, J., van Bellen, S., West, J. B., … Wu, J. (2020). Expert assessment of future vulnerability of the global peatland carbon sink. *Nature Climate Change*, *11*, 70–77. https://doi.org/10.1038/s41558-020-00944-0

Lund, M., LaFleur, P. M., Roulet, N. T., Lindroth, A., Christensen, T. R., Aurela, M., Chojnicki, B. H., Flanagan, L. B., Humphreys, E. R., Laurila, T., Oechel, W. C., Olejnik, J., Rinne, J., Schubert, P., & Nilsson, M. B. (2010). Variability in exchange of CO_2 across 12 northern peatland and tundra sites. *Global Change Biology*, *16*, 2436–2448. https://doi.org/10.1111/j.1365-2486.2009.02104.x

Lyu, Z., Genet, H., He, Y., Zhuang, Q., Breen, A., Clein, J., Euskirchen, E. S., Johnson, K., Kurkowski, T., Pastick, N., Rupp, T. S., Wylie, B., & Zhu, Z. (2018). The role of driving factors in historical and projected carbon dynamics in wetland ecosystems of Alaska. *Ecological Applications*, *28*, 1377–1395. https://doi.org/10.1002/eap.1755

Ma, S., Bloom, A. A., Watts, J. D., Quetin, G. R., Donatella, Z., Euskirchen, E. S., Norton, A. J., Yin, Y., Levine, P. A., Braghiere, R. K., & Parazoo, N. C. (2023). Resolving the carbon-climate feedback potential of wetland CO_2 and CH_4 fluxes in Alaska. *Global Biogeochemical Cycles*, *37*, e2022GB007524. https://doi.org/10.1029/2022GB007524

Manies, K. L., Dieleman, C., Douglas, T. A., James, S., McFarland, J., Minsley, B., Turetsky, M., & Waldrop, M. P. (2023). Depth to frozen soil measurements at APEX, 2008–2023. https://doi.org/10.5066/P92MAA6Z

Manies, K. L., Jones, M. C., Waldrop, M. P., Leewis, M.-C., Fuller, C., Cornman, R. S., & Hoefke, K. (2021). Influence of permafrost type

and site history on losses of permafrost carbon after thaw. *Journal of Geophysical Research: Biogeosciences*, *126*, e2021JG006396. https://doi.org/10.1029/2021JG006396

Massman, W. J. (2000). A simple method for estimating frequency response corrections for eddy covariance systems. *Agricultural and Forest Meteorology*, *104*, 185–198. https://doi.org/10.1016/S0168-1923(00)00164-7

Massman, W. J. (2001). Reply to comment by Rannik on "A simple method for estimating frequency response corrections for eddy covariance systems". *Agricultural and Forest Meteorology*, *107*, 247–251. https://doi.org/10.1016/S0168-1923(00)00237-9

McConnell, N. A., Turetsky, M. R., McGuire, A. D., Kane, E. S., Waldrop, M. P., & Harden, J. W. (2013). Controls on ecosystem and root respiration across a permafrost and wetland gradient in Interior Alaska. *Environmental Research Letters*, *8*, 045029. https://doi.org/10.1088/1748-9326/8/4/045029

McDermitt, D., Burba, G., Xu, L., Anderosn, T., Komissarov, A., Riensche, B., Schedlbauer, J., Starr, G., Zona, D., Oechel, W., Oberbauer, S., & Hastings, S. (2011). A new low-power, open-path instrument for measuring methane flux by eddy covariance. *Applied Physics B*, *102*, 391–405. https://doi.org/10.1007/s00340-010-4307-0

McPartland, M. Y., Kane, E. S., Falkowski, M. J., Kolka, R., Turetsky, M. R., Palik, B., & Montgomery, R. A. (2019). The response of boreal peatland community composition and NDVI to hydrologic change, warming, and elevated carbon dioxide. *Global Change Biology*, *25*, 93–107. https://doi.org/10.1111/gcb.14465

Mitchell, C. P. J., & Branfireun, B. A. (2005). Hydrogeomorphic controls on reduction-oxidation conditions across boreal upland-peatland interfaces. *Ecosystems*, *8*, 731–747. https://doi.org/10.1007/s10021-005-1792-9

Moore, T. R., & Roulet, N. T. (1993). Methane flux: Water table relations in northern wetlands. *Geophysical Research Letters*, *20*, 587–590. https://doi.org/10.1029/93GL00208

Myhre, G., Shindell, D., Bréon, F.-M., Collins, W., Fuglestvedt, J., Huang, J., Koch, D., Lamarque, J.-F., Lee, D., Mendoza, B., Nakajima, T., Robock, A., Stephens, G., Takemura, T., & Zhan, H. (2013). Anthropogenic & natural radiative forcing. In T. F. Stocker, D. Qin, G.-K. Plattner, M. Tignor, S. K. Allen, J. Boschung, A. Nauels, Y. Xia, V. Bex, & P. M. Midgle (Eds.), *Climate Change 2013: The physical science basis. Contribution of Working Group I to the fifth assessment report of the Intergovernmental Panel on Climate Change* (pp. 659–740). Cambridge University Press.

Nakai, T., Hiyama, T., Petrov, R., Kotani, A., Ohta, T., & Maximov, T. (2020). Application of an open-path eddy covariance methane flux measurement system to a larch forest in eastern Siberia. *Agricultural and Forest Meteorology*, *282-283*, 1–16. https://doi.org/10.1016/j.agrformet.2019.107860

Natali, S. M., Holdren, J. P., Rogers, B. M., Treharne, R., Duffy, P. B., Pomerance, R., & MacDonald, E. (2021). Permafrost carbon feedbacks threaten global climate goals. *Proceedings of the National Academy of Sciences of the United States of America*, *118*, e2100163118. https://doi.org/10.1073/pnas.2100163118

Natali, S. M., Watts, J. D., Rogers, B. M., Potter, S., Ludwig, S. M., Selbmann, A. K., Sullivan, P. F., Abbott, B. W., Arndt, K. A., Birch, L., Björkman, M. P., Bloom, A. A., Celis, G., Christensen, T. R., Christiansen, C. T., Commane, R., Cooper, E. J., Crill, P., Czimczik, C., … Zona, D. (2019). Large loss of CO_2 in winter observed across the northern permafrost region. *Nature Climate Change*, *9*, 852–857. https://doi.org/10.1038/s41558-019-0592-8

Neter, J., Kutner, M. H., Nachtsheim, C. J., & Wasserman, W. (1996). *Applied linear statistical models* (4th ed.). McGraw-Hill.

Neubauer, S. C., & Megonigal, J. P. (2015). Moving beyond global warming potentials to quantify the climatic role of ecosystems. *Ecosystems*, *18*, 1000–1013. https://doi.org/10.1007/s10021-015-9879-4

Neumann, R. B., Moorberg, C. J., Lundquist, J. D., Turner, J. C., Waldrop, M. P., McFarland, J. W., Euskirchen, E. S., Edgar, C. W., & Turetsky, M. R. (2019). Warming effects of spring rainfall increase methane emissions from thawing permafrost. *Geophysical Research Letters*, *46*, 1393–1401. https://doi.org/10.1029/2018GL081274

NOAA. (2021). NOAA webpage. https://www.ncei.noaa.gov/access/us-climate-normals/#dataset=normals-monthly&timeframe=30&location=AK&station=USW00026411

Olefeldt, D., Euskirchen, E. S., Harden, J., Kane, E. S., McGuire, A. D., Waldrop, M., & Turetsky, M. R. (2017). Greenhouse gas fluxes and their cumulative response to inter-annual variability and experimental manipulation of the water table position in a boreal fen. *Global Change Biology*, *23*, 2428–2440. https://doi.org/10.1111/gcb.13612

Overland, J. E. (2021). Rare events in the Arctic. *Climatic Change*, *168*, 27. https://doi.org/10.1007/s10584-021-03238-2

Overpeck, J., Hughen, K., Hardy, D., Bradley, R., Case, M., Finney, B., Gajwski, K., Jacoby, G., Jennings, A., Lamoureux, S., Lasca, A., MacDonald, G., Moore, J., Ratelle, M., Smith, S., Wolfe, A., & Zielinski, G. (1997). Arctic environmental change of the last four centuries. *Science*, *278*, 1251–1256. https://doi.org/10.1126/science.278.5341.1251

Papale, D., Reichstein, M., Aubinet, M., Canfora, E., Bernhofer, C., Kutsch, W., Longdoz, B., Rambal, S., Valentini, R., Vesala, T., & Yakir, D. (2006). Towards a standardized processing of net ecosystem exchange measured with eddy covariance technique: Algorithms and uncertainty estimation. *Biogeosciences*, *3*, 571–583. https://doi.org/10.5194/bg-3-571-2006

Peichl, M., Martínez-García, E., Fransson, J. E. S., Wallerman, J., Laudon, H., Lundmark, T., & Nilsson, M. B. (2023). Landscape-variability of the carbon balance across managed boreal forests. *Global Change Biology*, *29*, 1119–1132. https://doi.org/10.1111/gcb.16534

Pugh, C. A., Reed, D. E., Desai, A. R., & Sulman, B. N. (2017). Wetland flux controls: How does interacting water table levels and temperature influence carbon dioxide and methane fluxes in northern Wisconsin? *Biogeochemistry*, *137*, 15–25. https://doi.org/10.1007/s10533-017-0414-x

Pulliainen, J., Aurela, M., Vesala, T., Sonnentag, O., Lindroth, A., Aalto, T., Markkanen, T., Lemmetyinen, J., Thum, T., Derksen, C., Launiainen, S., Takala, M., Cohen, J., Salminen, M., Lindqvist, H., Böttcher, K., Rautiainen, K., Luojus, K., Pumpanen, J., … Kolari, P. (2022). Four decades increase in gross photosynthesis of boreal forests balanced out by increase in ecosystem respiration. *Research Square*. https://doi.org/10.21203/rs.3.rs-2308665/v1

Quinton, W. L., Hayashi, M., & Chasmer, L. (2011). Permafrost-thaw-induced land-cover change in the Canadian subarctic: Implications for water resources. *Hydrological Processes*, *25*, 152–158. https://doi.org/10.1002/hyp.7894

Reichstein, M., Falge, E., Baldocchi, D., Papale, D., Aubinet, M., Berbigier, P., Bernhofer, C., Buchmann, N., Gilmanov, T., Granier, A., Grünwald, T., Havránková, K., Ilvesniemi, H., Janous, D., Knohl, A., Laurila, T., Lohila, A., Loustau, D., Matteucci, G., … Valentini, R. (2005). On the separation of net ecosystem exchange into assimilation and ecosystem respiration: Review and improved algorithm. *Global Change Biology*, *11*, 1424–1439. https://doi.org/10.1111/j.1365-2486.2005.001002.x

Rinne, J., Tuittila, E.-S., Peltola, O., Li, X., Raivonen, M., Alekseychik, P., Haapanala, S., Pihlatie, M., Aurela, M., Mammarella, I., & Vesala, T. (2018). Temporal variation of ecosystem scale methane emission from a boreal fen in relation to temperature, water table position, and carbon dioxide fluxes. *Global Biogeochemical Cycles*, *32*, 1087–1106. https://doi.org/10.1029/2017GB005747

Roulet, N. T., Lafleur, P. M., Richard, P. J. H., Moore, T. R., Humphreys, E. R., & Bubier, J. (2007). Contemporary carbon balance and late Holocene carbon accumulation in a northern peatland. *Global Change Biology*, *13*, 397–411. https://doi.org/10.1111/j.1365-2486.2006.01292.x

Rupp, D., Kane, E. S., Dieleman, C., Keller, J. K., & Turetsky, M. R. (2019). Plant functional group effects on peat carbon cycling in a boreal

rich fen. *Biogeochemistry*, *144*, 305–327. https://doi.org/10.1007/s10533-019-00590-5

Rupp, D. L., Lamit, L. J., Techtmann, S. M., Kane, E. S., Lilleskov, E. A., & Turetsky, M. R. (2021). The rhizosphere responds: Rich fen peat and root microbial ecology after long-term water table manipulation. *Applied and Environmental Microbiology*, *87*, e0024121. https://doi.org/10.1128/AEM.00241-21

Schuur, E. A. G., Abbott, B., Commane, R., Ernakovich, J., Euskirchen, E. S., Hugelius, G., Grosse, G., Jones, M., Koven, C., Leyshk, V., Lawrence, D., Loranty, M., Mauritz, M., Olefeldt, D., Natali, S., Rodenhizer, H., Salmon, V., Schädel, C., Strauss, J., … Turetsky, M. (2022). Permafrost and climate change: Carbon cycle feedbacks from the warming Arctic. *Annual Review of Environment and Resources*, *47*, 343–371. https://doi.org/10.1146/annurev-environ-012220-011847

Sen, P. K. (1968). Estimates of the regression coefficient based on Kendall's tau. *Journal of the American Statistical Association*, *63*, 1379–1389. https://doi.org/10.1080/01621459.1968.10480934

Shur, Y. L., & Jorgenson, M. T. (2007). Patterns of permafrost formation and degradation in relation to climate and ecosystems. *Permafrost and Periglacial Processes*, *18*, 7–19. https://doi.org/10.1002/ppp.582

Strachan, I. B., Pelletier, L., & Bonneville, M. C. (2016). Inter-annual variability in water table depth controls net ecosystem carbon dioxide exchange in a boreal bog. *Biogeochemistry*, *127*, 99–111. https://doi.org/10.1007/s10533-015-0170-8

Strack, M., Mwakanyamale, K., Fard, G. H., Bird, M., Berube, V., & Rochefort, L. (2017). Effect of plant functional type on methane dynamics in a restored minerotrophic peatland. *Plant and Soil*, *410*, 231–246. https://doi.org/10.1007/s11104-016-2999-6

Tebaldi, C., Hayhoe, K., Armblaster, J. M., & Meehl, G. A. (2006). Going to the extremes: An intercomparison of model-simulated historical and future changes in extreme events. *Climatic Change*, *79*, 185–211. https://doi.org/10.1007/s10584-006-9051-4

Treat, C. C., & Jones, M. C. (2018). Near-surface permafrost aggradation in Northern Hemisphere peatlands shows regional and global trends during the past 6000 years. *The Holocene*, *28*, 998–1010. https://doi.org/10.1177/0959683617752858

Turetsky, M. R., Abbott, B. W., Jones, M. C., Anthony, K. W., Olefeldt, D., Schuur, E. A. G., Grosse, G., Kuhry, P., Hugelius, G., Koven, C., Lawrence, D. M., Gibson, C., Sannel, A. B. K., & McGuire, A. D. (2020). Carbon release through abrupt permafrost thaw. *Nature Geoscience*, *13*, 138–143. https://doi.org/10.1038/s41561-019-0526-0

Turetsky, M. R., Kotowska, A., Bubier, J., Dise, N. B., Crill, P., Hornibrook, E. R. C., Minkkinen, K., Moore, T. R., Myers-Smith, I. H., Nykänen, H., Olefeldt, D., Rinne, J., Saarnio, S., Shurpali, N., Tuittila, E. S., Waddington, J. M., White, J. R., Wickland, K. P., & Wilmking, M. (2014). A synthesis of methane emissions from 71 northern, temperate, and subtropical wetlands. *Global Change Biology*, *20*, 2183–2197. https://doi.org/10.1111/gcb.12580

Turetsky, M. R., Treat, C. C., Waldrop, M. P., Waddington, J. M., Harden, J. W., & McGuire, A. D. (2008). Short-term response of methane fluxes and methanogen activity to water table and soil warming manipulations in an Alaskan peatland. *Journal of Geophysical Research*, *113*, 1–15. https://doi.org/10.1029/2007JG000496

Turner, J. C., Moorberg, C. J., Wong, A., Shea, K., Waldrop, M. P., Turetsky, M. R., & Neumann, R. B. (2020). Getting to the root of plant-mediated methane emissions and oxidation in a thermokarst bog. *Journal of Geophysical Research: Biogeosciences*, *125*, e2020JG005825. https://doi.org/10.1029/2020JG005825

Ueyama, M., Harazono, Y., Ohtaki, E., & Miyata, A. (2006). Controlling factors on the inter-annual CO_2 budget at a sub-arctic black spruce forest in Interior Alaska. *Tellus*, *58*, 491. https://doi.org/10.1111/j.1600-0889.2006.00205.x

Ueyama, M., Ichii, K., Kobayashi, H., Kumagai, T'., Beringer, J., Merbold, L., Euskirchen, E. S., Hirano, T., Marchesini, L. B., Baldocchi, D., Saitoh, T. M., Mizoguchi, Y., Ono, K., Kim, J., Varlagin, A., Kang, M., Shimizu, T., Kosugi, Y., Bret-Harte, M. S., … Yasuda, Y. (2020). Inferring CO_2 fertilization effect based on global monitoring land-atmosphere exchange with a theoretical model. *Environmental Research Letters*, *15*, 084009. https://doi.org/10.1088/1748-9326/ab79e5

Ueyama, M., Iwata, H., & Harazono, Y. (2014). Autumn warming reduces the CO_2 sink of a black spruce forest in Interior Alaska based on a nine-year eddy covariance measurements. *Global Change Biology*, *20*, 1161–1173. https://doi.org/10.1111/gcb.12434

Van Cleve, K., Chapin, F. S., III, & Ruess, R. W. (2018). *Bonanza Creek LTER: Hourly precipitation weighing bucket measurements from 1988 to present in the Bonanza Creek Experimental Forest near Fairbanks, Alaska, Bonanza Creek LTER*. University of Alaska Fairbanks. BNZ:183, http://www.lter.uaf.edu/data/data-detail/id/183. https://doi.org/10.6073/pasta/1620b43e9ad1755b5d2001537aa13ad5

Virkkala, A.-M., Aalto, J., Rogers, B. M., Tagesson, T., Treat, C. C., Natali, S. M., Watts, J. D., Potter, S., Lehtonen, A., Mauritz, M., Schuur, E. A. G., Kochendorfer, J., Zona, D., Oechel, W., Kobayashi, H., Humphreys, E., Goeckede, M., Iwata, H., Lafleur, P. M., … Luoto, M. (2021). Statistical upscaling of ecosystem CO_2 fluxes across the terrestrial tundra and boreal domain: Regional patterns and uncertainties. *Global Change Biology*, *27*, 4040–4059. https://doi.org/10.1111/gcb.15659

Waldrop, M. P., Chabot, C. L., Liebner, S., Holm, S., Snyder, M. W., Dillon, M., Dudgeon, S. R., Douglas, T. A., Leewis, M. C., Walter Anthony, K. M., McFarland, J. W., Arp, C. D., Bondurant, A. C., Taş, N., & Mackelprang, R. (2023). Permafrost microbial communities and functional genes are structured by latitudinal and soil geochemical gradients. *The ISME Journal*, *17*, 1224–1235. https://doi.org/10.1038/s41396-023-01429-6

Waldrop, M. P., McFarland, J. W., Manies, K. L., Leewis, M. C., Blazewicz, S. J., Jones, M. C., Neumann, R. B., Keller, J. K., Cohen, L., Euskirchen, E. S., Edgar, C., Turetsky, M. R., & Cable, W. L. (2021). Carbon fluxes and microbial activities from boreal peatlands experiencing permafrost thaw. *Journal of Geophysical Research: Biogeosciences*, *126*, e2020JG005869. https://doi.org/10.1029/2020JG005869

Walsh, J. E., Bhatt, U. S., Littell, J. S., Leonawicz, M., Lindgren, M., Kurkowski, T. A., Bieniek, P. A., Thoman, R., Gray, S., & Rupp, T. S. (2018). Downscaling of climate model output for Alaskan stakeholders. *Environmental Modelling & Software*, *110*, 38–51. https://doi.org/10.1016/j.envsoft.2018.03.021

Watts, J. D., Farina, M., Kimball, J. S., Schiferl, L. D., Liu, Z., Arndt, K. A., Zona, D., Ballantyne, A., Euskirchen, E. S., Parmentier, F. J. W., Helbig, M., Sonnentag, O., Tagesson, T., Rinne, J., Ikawa, H., Ueyama, M., Kobayashi, H., Sachs, T., Nadeau, D. F., … Oechel, W. C. (2023). Carbon uptake in Eurasian boreal forests dominates the high-latitude net ecosystem carbon budget. *Global Change Biology*, *29*, 1870–1889. https://doi.org/10.1111/gcb.16553

Webb, E. K., Pearman, G. I., & Leuning, R. (1980). Correction of flux measurements for density effects due to heat and water vapour transfer. *Quarterly Journal of the Royal Meteorological Society*, *106*, 85–100. https://doi.org/10.1002/qj.49710644707

Wu, J., & Roulet, N. T. (2014). Climate change reduces the capacity of northern peatlands to absorb the atmospheric carbon dioxide: The different responses of bogs and fens. *Global Biogeochemical Cycles*, *28*, 1005–1024. https://doi.org/10.1002/2014GB004845

Wutzler, T., Lucas-Moffat, A., Migliavacca, M., Knauer, J., Sickel, K., Šigut, L., Menzer, O., & Reichstein, M. (2018). Basic and extensible post-processing of eddy covariance flux data with REddyProc. *Biogeosciences*, *15*, 5015–5030. https://doi.org/10.5194/bg-15-5015-2018

Yi, Y., Kimball, J. S., Rawlins, M. A., Moghaddam, M., & Euskirchen, E. S. (2015). The role of snow cover affecting boreal-arctic soil freeze–thaw and carbon dynamics. *Biogeosciences*, *12*, 5811–5829. https://doi.org/10.5194/bg-12-5811-2015

Zhang, H., Tuittila, E., Korrensalo, A., Laine, A., Uljas, S., Welti, N., Kerttula, J., Maljanen, M., Elliott, D., Vesala, T., & Lohila, A. (2021). Methane production and oxidation potentials along a fen-bog gradient from southern boreal to subarctic peatlands in Finland. *Global Change Biology*, *27*, 4449–4464. https://doi.org/10.1111/gcb.15740

Zhuang, Q., Wang, S., Zhao, B., Aires, F., Prigent, C., Yu, Z., Keller, J. K., & Bridgham, S. (2020). Modeling Holocene peatland carbon accumulation in North America. *Journal of Geophysical Research: Biogeosciences*, *125*, e2019JG005230. https://doi.org/10.1029/2019JG005230

Zoltai, S. C. (1972). Palsas and peat plateaus in central Manitoba and Saskatchewan. *Canadian Journal of Forest Research*, *2*, 291–302. https://doi.org/10.1139/x72-046

Zoltai, S. C. (1993). Cyclic development of permafrost in the peatlands of Northwestern Alberta, Canada. *Arctic, Antarctic, and Alpine Research*, *25*, 240–246.

Zona, D., Lafleur, P. M., Hufkens, K., Gioli, B., Bailey, B., Burba, G., Euskirchen, E. S., Watts, J. D., Arndt, K. A., Farina, M., Kimball, J. S., Heimann, M., Göckede, M., Pallandt, M., Christensen, T. R., Mastepanov, M., López-Blanco, E., Dolman, A. J., Commane, R., … Oechel, W. C. (2023). Pan-Arctic soil moisture control on tundra carbon sequestration and plant productivity. *Global Change Biology*, *29*, 1267–1281. https://doi.org/10.1111/gcb.16487

SUPPORTING INFORMATION

Additional supporting information can be found online in the Supporting Information section at the end of this article.

How to cite this article: Euskirchen, E. S., Edgar, C. W., Kane, E. S., Waldrop, M. P., Neumann, R. B., Manies, K. L., Douglas, T. A., Dieleman, C., Jones, M. C., & Turetsky, M. R. (2024). Persistent net release of carbon dioxide and methane from an Alaskan lowland boreal peatland complex. *Global Change Biology*, *30*, e17139. https://doi.org/10.1111/gcb.17139